MATERIALS SCIENCE

From room temperature to harsh temperature applications: Fundamentals and perspectives on electrolytes in zinc metal batteries

Sailin Liu[1]†, Ruizhi Zhang[2,3]†, Jianfeng Mao[1], Yunlong Zhao[4], Qiong Cai[2]*, Zaiping Guo[1,3]*

As one of the most competitive candidates for the next-generation energy storage systems, the emerging rechargeable zinc metal battery (ZMB) is inevitably influenced by beyond-room-temperature conditions, resulting in inferior performances. Although much attention has been paid to evaluating the performance of ZMBs under extreme temperatures in recent years, most academic electrolyte research has not provided adequate information about physical properties or practical testing protocols of their electrolytes, making it difficult to assess their true performance. The growing interest in ZMBs is calling for in-depth research on electrolyte behavior under harsh practical conditions, which has not been systematically reviewed yet. Hence, in this review, we first showcase the fundamentals behind the failure of ZMBs in terms of temperature influence and then present a comprehensive understanding of the current electrolyte strategies to improve battery performance at harsh temperatures. Last, we offer perspectives on the advance of ZMB electrolytes toward industrial application.

INTRODUCTION

Wide operational temperature ranges for energy storage systems are in urgent demand for electric vehicles, aerospace technology, and military and grid-scale utilization. The low redox potential of the Zn/Zn^{2+} couple (−0.76 V versus standard hydrogen electrode), high theoretical gravimetric/volumetric capacity (820 mA·hour g^{-1}/5855 mA·hour cm^{-3}), impressive electrochemical stability and reversibility, and its intrinsic safety and low toxicity have brought the zinc metal battery (ZMB) to the forefront of energy research. In particular, the ZMB is one of the few batteries where the metal anode can be successfully cycled in both aqueous and nonaqueous electrolytes. These merits make ZMBs attractive energy storage systems for a wide range of applications. Special practical applications, such as polar, aerospace, deep sea, and high-altitude region exploration, require the zinc-based energy storage device to operate at low or high temperatures. ZMBs, however, suffer from performance degradation and safety problems at extreme temperatures. At low temperatures (below 0°C), increased viscosity that leads to decreased ionic conductivity, as well as the liquid-to-solid phase transformation of the electrolyte, is hindering its practical application (*1*–*3*). At high temperatures (over 25°C), the use of commonly adopted aqueous electrolytes in ZMBs is also limited by the highly volatile nature of water and the instability of the electrolyte/electrode interface.

To achieve ultralow-temperature operation for ZMBs, it is necessary to address two issues: the high freezing point and the low ionic conductivity of the electrolyte under subzero temperature conditions. Compared to nonaqueous electrolytes, water-based electrolytes offer high conductivity but are limited by their high freezing point. In general, there are two well-established ways to extend the temperature range of the aqueous electrolyte: (i) using organics to form eutectics or antifreezing hydrogels and (ii) using concentrated electrolyte with a high ratio of salt to water (*4*). Although the highly concentrated "water-in-salt" (WIS) strategy could notably lower the freezing point of aqueous electrolytes, it introduces the disadvantages of high viscosity and low conductivity and increased costs. Strategies for hydrogels that contain aqueous electrolytes are commonly reported with wide workable temperature windows due to the low-freezing point of cross-linked gels or interference from the boundaries between the gel and the water. Organic solvents could be used in dilute concentrations and tend to have a much lower freezing point than water, showing their potential as good candidates for subzero application. Most of the organic solvents, however, have insufficient ionic conductivity compared to water and could possibly sacrifice the intrinsic safety properties of the ZMBs due to their highly flammable nature. The recent studies on organic solvents that are miscible with water offer prospects for designing hybrid electrolytes with extended temperature ranges. By taking advantages of the various merits of both water and organics, the hybrid liquid electrolytes, such as dimethyl sulfoxide (DMSO) and triethyl phosphate (TEP), not only showcase better thermal stability but also have a protective effect on electrodes (*5*, *6*). Inspired by the research on Li metal batteries, there are now various studies and reviews on electrolytes and anodes to address the Zn metal dendrite and H-evolution issues. The recent works on concentrated electrolytes, such as 7.6-m $ZnCl_2/H_2O$ with 0.05-m $SnCl_2$, show that they could not only form a $Zn_5(OH)_8Cl_2{\cdot}H_2O$ solid-electrolyte interphase (SEI) on metal anode surface to suppress Zn dendrite growth but also present high ionic conductivity at −70°C.

The massive achievements gained by electrolyte studies exhibit the importance of electrolytes for the whole battery performance, which calls for specific reviews on the different aspects. The flourishing innovations on electrolytes are usually targeted on addressing the issues from the viewpoint of electrolyte/electrode interface, extending the working voltage range, or improving the temperature

[1]School of Chemical Engineering and Advanced Materials, University of Adelaide, Adelaide, SA 5005, Australia. [2]Department of Chemical and Process Engineering, Faculty of Engineering and Physical Sciences, University of Surrey, Guildford, Surrey GU2 7XH, UK. [3]The Institute for Superconducting and Electronic Materials, The Australian Institute for Innovative Materials, University of Wollongong, Wollongong, NSW 2500, Australia. [4]Advanced Technology Institute, Department of Electrical and Electronic Engineering, University of Surrey, Guildford, Surrey GU2 7XH, UK.
*Corresponding author. Email: zaiping.guo@adelaide.edu.au (Z.G.); q.cai@surrey.ac.uk (Q.C.)
†These authors contributed equally to this work.

adaptability. To date, there have been sufficient reviews on summarizing the progress on issues for the cathode/anode and a few reviews on guiding electrolyte design toward stable interfaces for ZMBs. There is a lack of reviews on the principles of electrolyte design and the prospects for electrolytes suitable for challenging applications under harsh temperature conditions. There are many research works that provide experimental results on electrolyte performance under all temperatures, but most of them fail to give their full physical properties, such as their ionic conductivity and freezing point. Hence, future studies on the improvement of electrolyte performance beyond room temperature require a comprehensive review of electrolyte development from the temperature aspect. In this review, we reveal the fundamentals behind the temperature as a cause of battery failure and recommend design principles according to the electrolyte type (water-based and all-organic electrolytes) and temperature. Accordingly, the current progress on the four main strategies is thoroughly discussed and compared: high salt-to-solvent ratio, additives/cosolvents (additive and cosolvent strategies are generally referred to as adopting a small and a large nonaqueous solvent-to-water volume/weight ratio, respectively), and all-organic and hydrogel.

THE FUNDAMENTALS BEHIND ANTIFREEZING STRATEGIES AND HIGH TEMPERATURE USE

In general, apart from the costly ionic liquid- and solid-state electrolytes, the electrolyte normally consists of water or an organic solvent. Therefore, a thorough review on water-based and organic electrolytes is provided from the fundamentals to general design principles.

The performance of batteries is acknowledged to be affected by the variation of temperature, which appears as the deterioration of rate capacities and cycling life beyond comfortable indoor degrees. Under cold conditions, as schematically illustrated in Fig. 1, the electrolytes are mainly subject to inefficient ionic conductivity and increased viscosity and charge transfer resistance, resulting in the deterioration of rate performance (*7*, *8*). If the temperature reaches the freezing point of the electrolyte, then crystallization will occur that can lead to volume expansion of the electrolyte and interfacial separation between electrolyte and electrode. Above room temperature, the inferior thermal and interfacial stabilities also pose a challenge to most of the ZMBs regarding safe and long-term operation. Although the aqueous electrolytes are good options for a noncombustible battery, most of them have poor stability under high temperatures due to the enhanced activity of water molecules. The extreme heat inside the battery will accelerate the side reactions of water with both electrodes, which may lead to structural damage or phase changes in the cathode and depletion of the zinc metal anode, as illustrated in Fig. 1. Since some active materials, such as the dominant manganese- and vanadium-based oxides, suffer from a dissolution problem in aqueous electrolytes, the high temperature can encourage these adverse reactions and cause irreversible destruction. Compared with the safe aqueous electrolytes, the electrolytes that use organic solvents with high flammability and low boiling points are not ideal for ZMBs. The failure of organic solvent–based batteries to work under high temperature usually follows the typical thermal runaway process, where the accumulated heat causes unfavorable exothermic reactions between the cathode and the electrolyte. The cathode, cathode electrolyte interphase (CEI) and SEI can further decompose and release flammable hydrocarbon gases and oxygen, encouraging combustion. Besides the above-complicated reactions, most organic electrolytes are characterized by high volatility, which will increase the pressure inside the battery and further cause battery swelling or explosion. In view of these challenges from harsh temperatures, it is important to find the underlying key factors that determine the electrolyte properties and accordingly propose strategies for wide temperature applications.

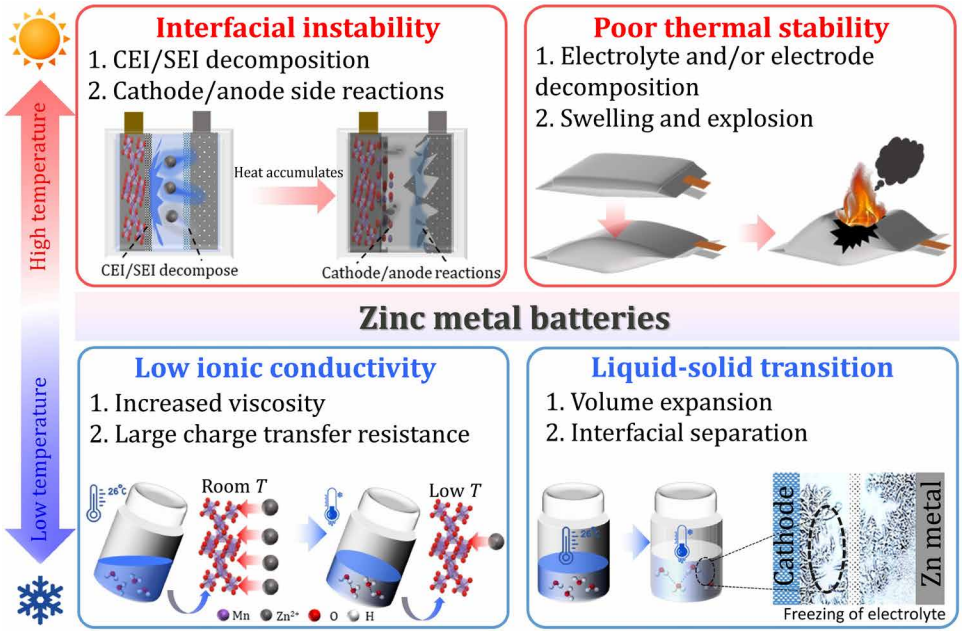

Fig. 1. Summary of the main challenges on electrolytes when using ZMBs at harsh temperatures. The main issues and failure reasons of electrolytes in ZMBs under subzero or over room temperature condition.

For water-based electrolytes, the inefficient ionic conductivity and freezing characteristics of water-based electrolytes under subzero temperatures are affected by the hydrogen bonds (HBs) between water molecules, which become stronger when the temperature decreases (*9*). A general way to increase the low-temperature performance is weakening the H—O bond strength or suppressing the formation of HBs in water. In this respect, as briefly described in Fig. 2, four fundamental routes have been proposed by researchers: (i) adopt anions that contain H-bonding acceptor elements, such as nitrogen (N), oxygen (O), or fluorine (F); (ii) use a concentrated electrolyte solution, where abundant ions are introduced to bond with water and compete with the original H—O bonding between water molecules; (iii) bring in additives/cosolvents to generate new HBs with water; and (iv) use hydrophilic polymer chains to create a cross-linked meshwork with water. On the other hand, to suit the demand for safe and long-term cycling above room temperature, the main principle is to increase the thermal stability of the electrolyte by minimizing its volatility and controlling decomposition. By diminishing the content of water, the boiling point of the electrolyte could be increased, and a wide range of approaches, such as highly concentrated, nonaqueous/aqueous hybrid solvents and hydrogels, have been established on this principle. To further enhance the high-temperature tolerance of the electrolyte, the salt is also required to show high thermal stability, which means that it is difficult to decompose at high temperatures.

Although the organic solvent–based electrolyte usually shows a much lower freezing point and broader operational voltage window than the aqueous electrolyte, it has the intrinsic disadvantage of low ionic conductivity at room temperature, which is unfavorable to fast charging (*10*, *11*). The cold conditions will further weaken the performance of a battery with an organic electrolyte, since the ionic conductivity will be greatly diminished when the temperature decreases to subzero. Therefore, the crucial approach to enhancing the low-temperature performance of organic electrolytes is to increase their ionic conductivity, which is determined by the affinity between the organic solvent and the ions (*7*, *12*). A strong affinity between the solvent and zinc ions will increase the difficulty of cation desolvation and thus reduce the ionic conductivity. Therefore, to reduce the affinity, strategies are usually proposed that require the solvent to have low viscosity or a low melting point (T_m), or the salt to have high solubility. To expand the working range of organic electrolytes toward higher temperatures, the main solution is to reduce the volatility and flammability of the solvents, which includes strategies for using concentrated electrolyte to reduce the solvent ratio or adopting the solvents with low volatility, such as fire retardants with wide thermal stability ranges.

DISCUSSION OF THE DEVELOPMENT OF THE CURRENT STRATEGIES

Overview of the electrolytes for wide temperature applications in ZMBs

Intensive research on ZMBs has been rapid over the past several decades, but the study of its wide temperature operation is still in its

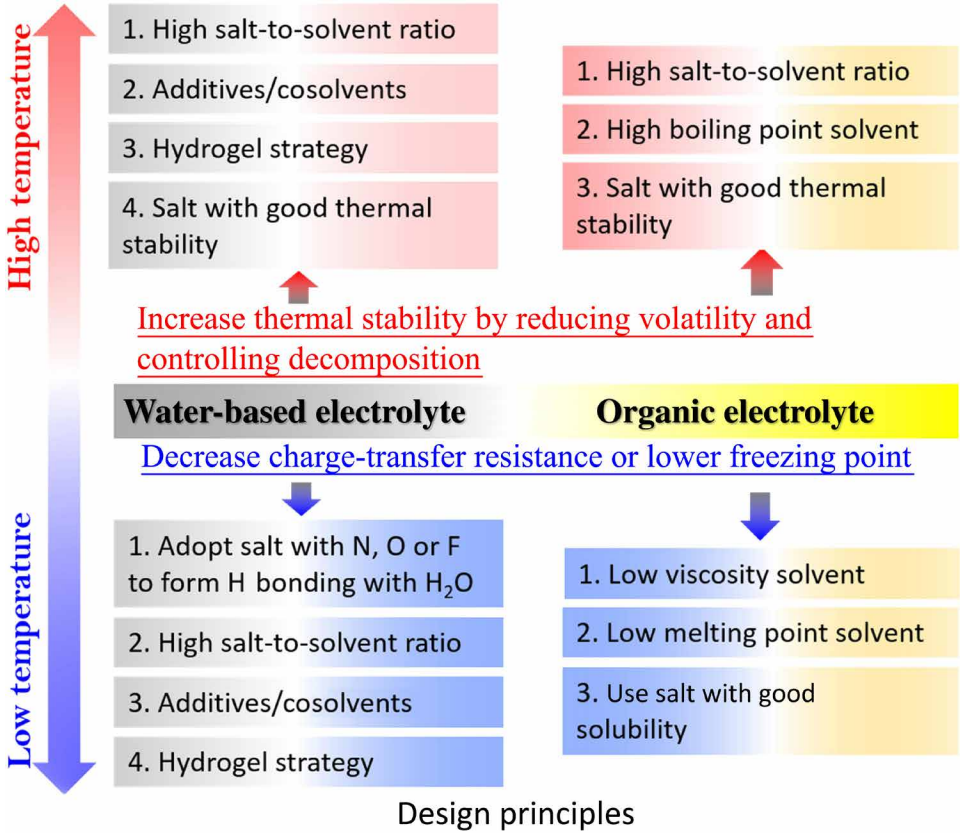

Fig. 2. Electrolyte design principles for ZMBs toward extreme temperature application. Fundamentals of electrolyte design for low-temperature and high-temperature use and related strategies for water-based and organic solvent–based nonaqueous electrolytes.

infancy stage. As seen in Fig. 3, since 2018, a few representative electrolytes with different zinc salts were developed with remarkable temperature adaptability. In the initial report on concentrated aqueous electrolyte using 3 M of $Zn(OTf)_2/H_2O$, where OTf^- is trifluoromethanesulfonate, it was found to have an operational temperature between −10° and 50°C (*13*). $ZnSO_4/H_2O$ electrolyte with a concentration of 2 M was reported to have a workable range of 0° to 50°C (*14*, *15*). In the following years, notable progress was made on extending the operational temperature range and improving the ionic conductivity of aqueous electrolytes under subzero temperatures. Concentrated 7.5 M $ZnCl_2/H_2O$ electrolyte presented an adequate ionic conductivity of 1.79 mS cm^{-1} at −60°C and a wide liquid range from −90° to 60°C (*1*). $Zn(BF_4)_2$ aqueous electrolyte (4 M) also exhibited a superb low temperature working ability down to −95°C (*16*). $Zn(TFSI)_2$ salt at a concentration of 4 M in water featured an impressive high ionic conductivity of 90 mS cm^{-1} (*17*). The high conductivity and safety merits of aqueous electrolytes are well preserved in the hydrogel electrolytes. A quasi–solid-state hydrogel based on 3 M $Zn(OTf)_2$/polyacrylamide (PAM) presented a workable temperature range of −30° to 80°C (*18*). Another hydrogel electrolyte based on different gels or multiple salts, such as cellulose/TEOS/glycerol(CT3G30)/2 M $ZnSO_4$/0.2 M $MnSO_4$, where TEOS is tetraethyl orthosilicate, A-PAA–30 weight % (wt %) KOH/H_2O, where A-PAA is alkalified poly(acrylic acid), and zinc alginate gel, can exhibit high ionic conductivity of 19.4 mS cm^{-1} at −40°C, 24.1 mS cm^{-1} at −20°C, and 32.3 mS cm^{-1} at 25°C, respectively (*19*–*21*). Recently, organic electrolytes using DMF (dielectric constant, ε = 36.7) and AN (ε = 37.5), where DMF is dimethylformamide and AN is acetonitrile, are reported to have wide working temperature ranges of −70° to 150°C and −40° to 80°C, respectively (*11*, *22*). Introducing an organic cosolvent into water to form a hybrid electrolyte has also received great attention because of the protective effect on the

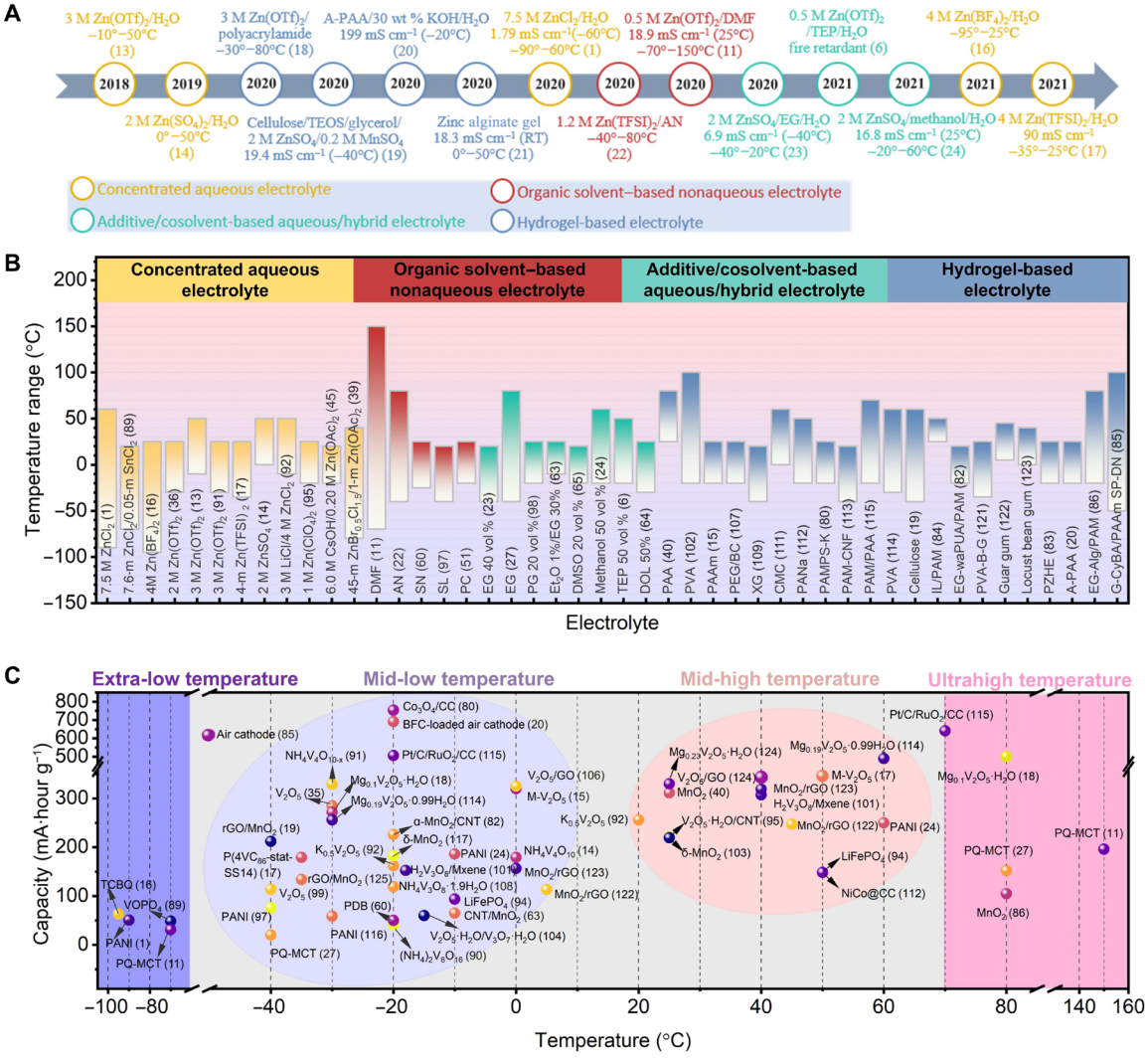

Fig. 3. Summary of advanced electrolytes and cathode materials in ZMBs for beyond-room-temperature use. (**A**) Roadmap of representative progress on electrolytes in ZMBs for harsh temperature applications. (**B**) The working temperature ranges of the reported concentrated aqueous electrolyte, organic solvent–based nonaqueous electrolyte, additive/cosolvent-based aqueous/hybrid electrolyte, and hydrogel-based electrolyte. (**C**) The capacities of the reported cathode materials under various temperatures. The extra-low, mid-low, mid-high, and ultrahigh temperature range represents temperature that is lower than −40°C, within −40° to 10°C, within 20° to 60°C, and higher than 60°C, respectively.

metal anode, the good temperature adaptability, etc. $ZnSO_4$/EG/H_2O (2 M) (*23*), where EG is ethylene glycol, and 2 M $ZnSO_4$/methanol (MeOH)/H_2O (*24*) electrolytes were found to have superb ionic conductivities of 6.9 mS cm^{-1} at −40°C and 16.8 mS cm^{-1} at room temperature, respectively. Since most of the reported organic cosolvents are highly flammable, fire-retardant phosphates (*25*, *26*) have been recently introduced. Adopting TEP as cosolvent is found to be anode friendly, which can assist in generating a robust SEI and reducing the volatility of the electrolyte by forming strong bonding with water molecules (*6*).

The reported electrolytes for harsh temperature use can be categorized into four classes: concentrated aqueous electrolytes, organic solvent–based nonaqueous electrolytes, water-based electrolytes with additives/cosolvents, and hydrogel electrolytes, according to their composition. To date, extensive efforts have been made toward expanding the temperature range in these four categories, as compared in Fig. 3B. It can be seen that most of the concentrated electrolytes have been reported with good low-temperature flexibility but relatively insufficient high-temperature suitability. In concentrated aqueous electrolyte, the top two extra-low-temperature performances that have been achieved were with 4 M $Zn(BF_4)_2$/H_2O and 7.5 M $ZnCl_2$/H_2O, approaching −100°C, while the highest temperature reported is 60°C for 7.5 M $ZnCl_2$/H_2O (*1*, *16*). The aqueous electrolytes with mid-high concentrations, such as 2 M $ZnSO_4$/H_2O and 3 M $Zn(OTf)_2$/H_2O, were reported to work within the range of 0° to 50°C and −10° to 50°C, respectively (*13*–*15*). The single organic solvent–based electrolytes are showing good prospects, since a few solvents, such as DMF and AN, can work in wide temperature windows, but most of the reported organic electrolytes have limited working temperature ranges, possibly because of their strong affinity to the ions or their high volatility (*7*). Using a certain proportion of organic solvents as additives or cosolvents to mix with water is an encouraging method for extending the temperature window of aqueous electrolytes. EG and poly(ethylene glycol) (PEG) have received great attention because of their high miscibility in water, and the highest temperature range achieved was with 50 volume % EG with a reported range of −40° to 80°C (*27*). For utilization under various temperatures, most of the attention has been paid to the hydrogel electrolytes. The lowest temperature reported, however, is limited to above −50°C, which is possibly due to the large amount of water in the cross-links of the gel.

Other than the electrolytes, the electrode materials also affect the battery performance under harsh temperatures, as summarized in Fig. 3B. For low-temperature application, most materials are reported to perform within the mid-low temperature range (−40° to 10°C). Under extra-low temperatures (lower than −40°C), a very limited number of materials have been studied, and apart from an air cathode that maintained a high capacity of over 600 mA·hour g^{-1} (−50°C), the capacities of most materials are usually below 100 mA·hour g^{-1}. Raising the temperature above room temperature can yield higher capacity than in the low temperature range. The Mn- and V-based cathodes, such as MnO_2 and $Mn_xV_2O_5$, can work effectively within a generally broad temperature window (mid-low and mid-high temperature ranges), showing potential for application in wider ranges. The organic materials, such as polyaniline (PANI) and phenanthrenequinone macrocyclic trimer (PQ-MCT) are reported to work at extra-low and extra-high temperatures, but they present unappealing capacities. The performance of cathodes in Fig. 3C may partly reflect the working ability of the materials due to the differences in the electrolytes and testing protocols, and it is believed that the energy density of the reported materials could still be improved in combination with the proper electrolytes.

DISCUSSION

At subzero temperature, insufficient ionic conductivity of the electrolyte and slow migration of ions result in poor energy and power density. Freezing of the electrolyte impairs the contact between the electrode and the electrolyte, causing higher interface resistance and even battery failure (*28*). At high temperature, fast volatilization of the solvent induces swelling of the battery and precipitation of the salt, greatly affecting the stability of batteries (*29*). In terms of the aqueous electrolyte, unordered water is transformed into ordered ice, and the process is driven by extra HB formation. During the volatilization of water, HBs between water molecules are broken (*8*, *30*). Thus, adding components that are capable of modulating HBs in the solution is a general strategy to change the freezing/boiling point. To minimize the negative effect of freezing/volatilization on the electrolyte, other methods such as reducing the water content and substituting weak volatile solvents for water have been adopted for the design of ZMBs with wide operating temperature ranges. In this section, we will discuss the development of different classes of electrolytes will be discussed in more detail.

Concentrated aqueous electrolyte

Increasing the concentration of salts is an efficient way to decrease the freezing point of a solution. The interaction between ions and water molecules enlarges the distance between water molecules and reduces the number of HBs between water molecules, effectively lowering the freezing point (*31*).

More HBs are destroyed when the concentration of salt (C_{salt}) increases, and thus, highly soluble salts such as $ZnCl_2$ (432 g/100 g at 25°C) are preferred. However, if the C_{salt} exceeds a certain value, then the interaction between anions and cations will be strengthened, which is detrimental to mass transfer and can increase the liquid-solid transition temperature (T_t) (*1*). The balance between HBs and ion interactions was achieved by varying C_{ZnCl2}, as shown in Fig. 4A. The T_t of a $ZnCl_2$ solution was lowered to −114°C with a C_{ZnCl2} of 7.5 m in Fig. 4B, enabling a Zn||PANI battery to operate from −90° to 60°C (*1*). In addition to high solubility, the intrinsic properties of the anion and cation should be noted. Elements such as nitrogen (N), oxygen (O), and fluorine (F) are HB acceptors and can easily form HBs (O—H···X) with water molecules (*32*–*34*). Fourier transform infrared spectroscopy (FTIR) investigations (as shown in Fig. 4, C and D) and the ratio of different HBs in Fig. 4E indicate the intensification of weak OH···F HBs between water molecules and BF_4^- anions and the weakening of strong OH···O HBs between water molecules, when $C_{Zn(BF4)2}$ increases from 1 M to 4 M. BF_4^- anions were proved to damage the original HB network within water and hinder ice nucleation. A 4 M $Zn(BF_4)_2$-based electrolyte achieved a low freezing point (−122°C) and a high ion conductivity (1.47 mS cm^{-1} at −70°C) and enabled the Zn||tetrachlorobenzoquinone (TCBQ) battery to reach a discharge capacity of 63.5 mA·hour g^{-1} at −95°C within a wide operating temperature range from −95° to 25°C (*16*). Correlations and effects of the cation-water, anion-water, and cation-anion interactions, as shown in Fig. 4F, were investigated through five commonly used Zn salts including $ZnSO_4$, $Zn(NO_3)_2$, $ZnCl_2$, ZnI_2, and $Zn(OTf)_2$. It is summarized in Fig. 4G that an anion with high

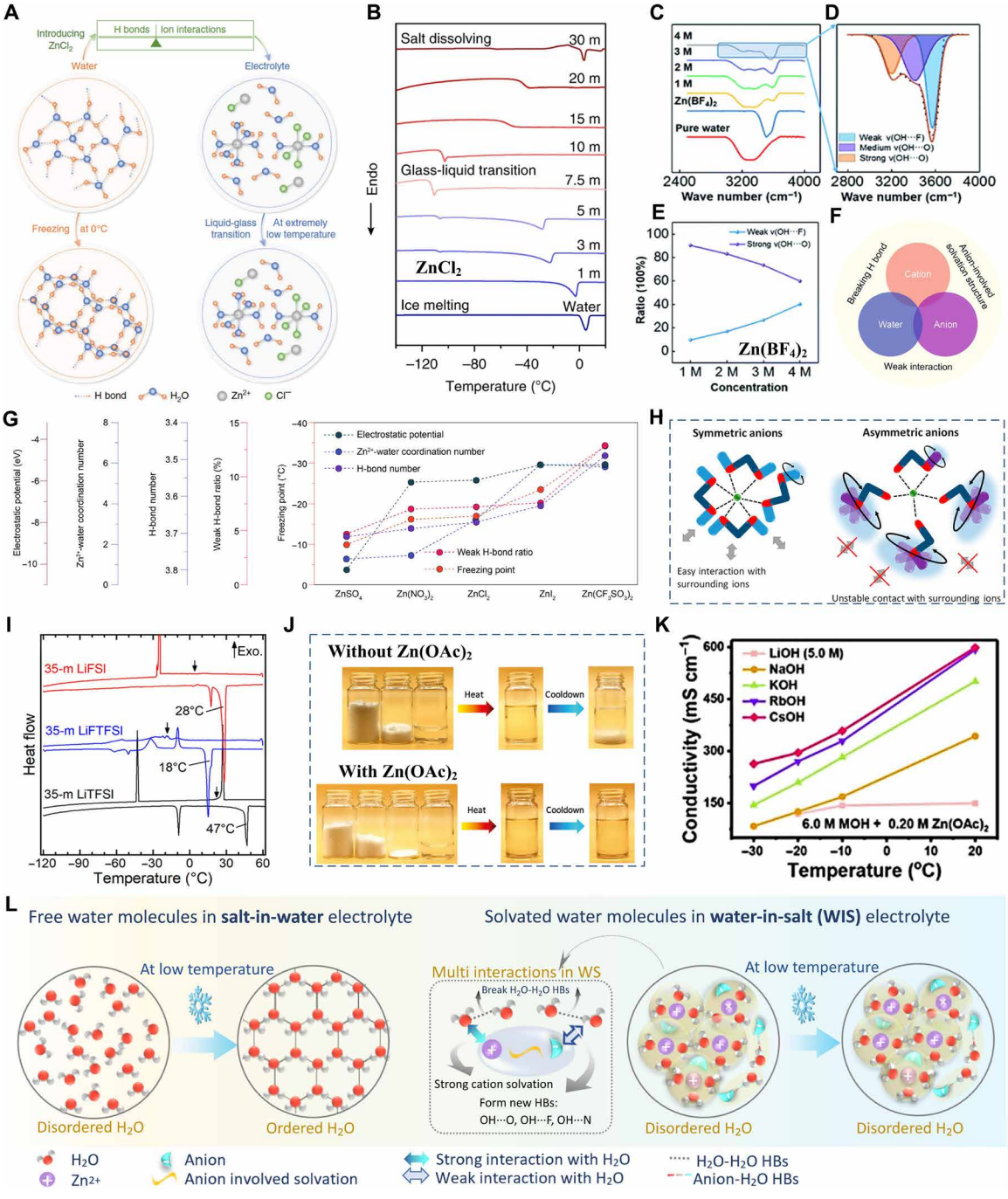

Fig. 4. Summary of recent advances on antifreezing concentrated aqueous electrolytes and the illustration of the antifreezing mechanism. (**A**) Schematic illustration of the structural evolution of water and electrolyte, and the design of a low-T_t solution. (**B**) Differential scanning calorimetry (DSC) test of different concentrations of $ZnCl_2$ from −150° to 20°C. (A) and (B) are reproduced with permission from Springer Nature (*1*). (**C**) FTIR spectra for O—H bonds of pure water, $Zn(BF_4)_2$, and 1 to 4 M $Zn(BF_4)_2$. (**D**) The fitted O—H stretching vibration. (**E**) The ratio of weak OH···F to strong OH···O HBs. (C) to (E) are reproduced with permission from the Royal Society of Chemistry (*16*). (**F**) Correlations and effects of the cation-water, cation-anion, and anion-water interactions. (**G**) Summary of the correlations among the characteristics of electrolytes, including the electrostatic potential, Zn^{2+}-water coordination number, HB number, weak HB ratio, and freezing point. (F) and (G) are reproduced with permission from the American Chemical Society (*35*). (**H**) Schematic illustration of the difference in local coordination for symmetric $TFSI^-$ and asymmetric $FTFSI^-$ anions. (**I**) DSC cooling and heating curves of 35-m LiFSI, LiFTFSI, and LiTFSI. (H) and (I) are reproduced with permission from the American Chemical Society (*38*). (**J**) Optical images of 40 m $ZnBr_{0.5}Cl_{1.5}$ suspension [without $Zn(OAc)_2$] and WSOE45-1 [with $Zn(OAc)_2$]. Reproduced with permission from John Wiley and Sons (*39*). (**K**) Ionic conductivity of electrolytes with various alkali metal cations. Reproduced with permission from John Wiley and Sons (*45*). (**L**) Schematic illustration of interactions around water molecules in salt-in-water and water-in-salt electrolytes at low temperature.

electrostatic potential generates a weak Zn^{2+}-anion interaction and a high Zn-water coordination number, resulting in a small HB number in molecular dynamics simulations, a low HB intensity in FTIR, and a lower freezing point (*35*).

Asymmetric anions have been proved to be capable of preventing the crystallization of WIS electrolytes at low temperatures (*36*–*38*). WIS electrolytes based on asymmetric (fluorosulfonyl) (trifluoromethanesulfonyl)imide ($FTFSI^-$) anions, as well as its symmetric anion analogs bis(fluorosulfonyl)imide (FSI^-) anion and bis(trifluoromethanesulfonyl)imide ($TFSI^-$) anion, were investigated in terms of the local solution structures and dynamic behavior. Figure 4H compares the local coordination for symmetric $TFSI^-$ and asymmetric $FTFSI^-$ anions. Uncoordinated SO_2CF_3 groups in $FTFSI^-$ with high rotational mobility impede close packing of the surrounding ions. Asymmetry also increased the difficulty of forming ordered arrangements of electrolyte species. Therefore, the crystallization process was suppressed, and asymmetric LiFTFSI-based electrolyte exhibited the lowest freezing point of −18°C, as shown in Fig. 4I (*38*).

Recently, the physical solubility limit of salts in water was broken by adding acetate anions, and the nonpolarized protons could prevent the overgrowth and precipitation of ionic oligomers (*39*, *40*). $ZnCl_2/ZnBr_2/Zn(OAc)_2$-based aqueous electrolyte, where OAc^- stands for acetoxy group, reached a record-breaking solubility of 75 m, far exceeding those of water-in-(bi)salt/hydrate melt electrolytes (21 to 40 m) (*41*–*44*). In a 40-m $ZnBr_{0.5}Cl_{1.5}$ aqueous solution [without $Zn(OAc)_2$], salt precipitation occurred, while the WSOE45-1 sample [45-m $ZnBr_{0.5}Cl_{1.5}$ and 1-m $Zn(OAc)_2$] was stable after cooling down in Fig. 4J. Furthermore, no salt crystallization or water freezing was observed from 40° to −80°C, suggesting the high concentration and antifreezing property of WSOE45-1 (*39*).

In addition to the freezing point, ionic conductivity at low temperature is a vital property as well. A series of alkaline electrolytes containing 6 M MOH and 0.2 M $Zn(OAc)_2$ (M = Li, Na, K, Rb, Cs; 5.0 M LiOH) were investigated, and they all remained liquid at −30°C except for the LiOH-based electrolyte. In Fig. 4K, ionic conductivity follows the sequence of Cs > Rb > K > Na > Li. The apparent high conductivity of CsOH-based electrolyte could be ascribed to the sparse solvation structure of the cations with a larger atomic number, which allowed more free ions to migrate (*45*).

The concentrated electrolyte strategy has attracted much attention because of the following advantages: (i) decreasing the freezing point of the electrolyte (*1*), (ii) expanding the electrochemical stability window of the electrolyte (*46*), (iii) alleviating the dissolution of the cathode and corrosion of the anode (*47*), (iv) accelerating electrode reactions (*48*), and (v) increasing the metal ion transference number (*49*). All these merits endow the ZMB with splendid electrochemical performance at low temperatures. Figure 4L illustrates the free water molecules in salt-in-water electrolyte and solvated water molecules in water-in-salt electrolyte. There are two main interactions that affect the H_2O-H_2O HBs: the Zn ion-H_2O and anion-H_2O interactions. The solvation force of Zn^{2+} with water is known as the strongest interaction, but its solvating ability is influenced by the type of anions. An anion with a higher electrostatic potential can lead to a larger zinc-H_2O coordination number (*35*). Although not as strong as the Zn ion-H_2O solvating force, the anion-H_2O interaction due to the formation of new HBs through the HB-acceptor elements (O, F, and N) has also been found to lower the electrolyte freezing point. To summarize, salts with the following characteristics are promising candidates: (i) high solubility (*1*), (ii) forming HBs with water molecules (*17*, *35*), and (iii) inhibiting ions or the solvent from forming long-range order (*39*, *40*). Nevertheless, the limitations of the concentrated electrolyte strategy should not be neglected, including (i) high viscosity due to the strong cation-anion ion coupling, (ii) low ionic conductivity, (iii) crystal precipitation, and (iv) high cost due to using a large amount of expensive salt (e.g., fluorinated salt).

Organic solvent–based nonaqueous electrolytes

Replacing water with organic solvents that have low freezing points such as DMF, AN, and propylene carbonate (PC) is an effective way to enhance the performance of the electrolyte at low temperatures. DMF is a polar solvent with a low freezing point (−61.4°C), a high boiling point (153°C), and high dielectric constant (36.7), which is used as an additive or solvent for electrolytes (*50*). In Fig. 5 (A and B), the freezing point of 0.5 M $Zn(OTf)_2$/DMF is −70.8°C, enabling Zn||PQ-MCT cells to reach capacity retention rates with 66.2% (−40°C) and 23.8% (−70°C) of the capacity at room temperature. In addition, the Zn^{2+}-DMF complex enhanced zinc salt solubility, suppressed growth of dendrites, and completely avoided the unwanted side effects caused by water, such as the hydrogen evolution reaction and corrosion of zinc anode (*11*). Common organic solvents with wide liquid temperature ranges, such as AN (*22*) (−45° to 81.6°C) and PC (*51*–*53*) (−48.8° to 242°C), are also used as antifreeze in ZMBs. A Zn/graphite battery with 1.2 M $Zn(TFSI)_2$/AN electrolyte operated from −40° to 80°C, and no obvious capacity fading was observed after 400 cycles at −40°C (*22*). A $Zn||Zn(ClO_4)_2/PC||Mn_{0.15}V_2O_5{\cdot}nH_2O$ cell achieved a specific capacity of 100 mA·hour g^{-1} after 3000 cycles at −20°C, as shown in Fig. 5C (*52*).

Binary and ternary solvent systems have been developed for ZMBs at room temperature to achieve enhanced electrochemical stability and zinc anode reversibility. Trimethyl phosphate (TMP) was introduced into ethyl methyl carbonate (EMC), and the anion solvation network notably increased the oxidation stability of electrolyte from 2.55 to 3.00 V (versus Zn/Zn^{2+}) as shown in Fig. 5D. Batteries based on $Zn(TFSI)_2$/EMC-TMP (1:3 by volume) electrolyte exhibited excellent cyclability and capacity, as seen in Fig. 5E (*54*). Qiu *et al.* (*55*) optimized the PC/TEP ratio in their organic electrolyte, and the electrolyte showed a high conductivity, a wide stable potential window, and the capability to suppress dendrite growth. In recent years, the electrochemical performance of lithium-ion batteries (LIBs) at low temperatures has been enhanced by changing the composition of solvent mixtures (*56*–*59*). For example, the ternary ethylene carbonate–PC-EMC (EC-PC-EMC) solvent system with optimized EC content allowed a 1 A·hour graphite||$LiNi_{1/3}Mn_{1/3}Co_{1/3}O_2$ pouch cell to exhibit outstanding long-term cycling performance at −30°C (*56*). Inspired by the design of LIBs for low temperatures and the fact that melting points of EMC (−55°C), TMP (−46°C), PC (−48.8°C), and TEP (−56.5°C) are all below zero, there is great potential to develop mixed organic solvent–based electrolytes to prevent freezing in zinc ion batteries, and not much work has been done in this area.

Using an organic solvent with a low freezing point is a straightforward method to fabricate antifreezing ZMBs. However, this does not mean that solvents with a high melting point have no chance to serve as the solvent. Succinonitrile (SN) exhibits a plastic-crystal phase at room temperature with a T_m of 54° to 57°C. By surrounding the nitrile with water dipoles, the intense nitrile-nitrile dipolar associations responsible for the regular long-range crystalline

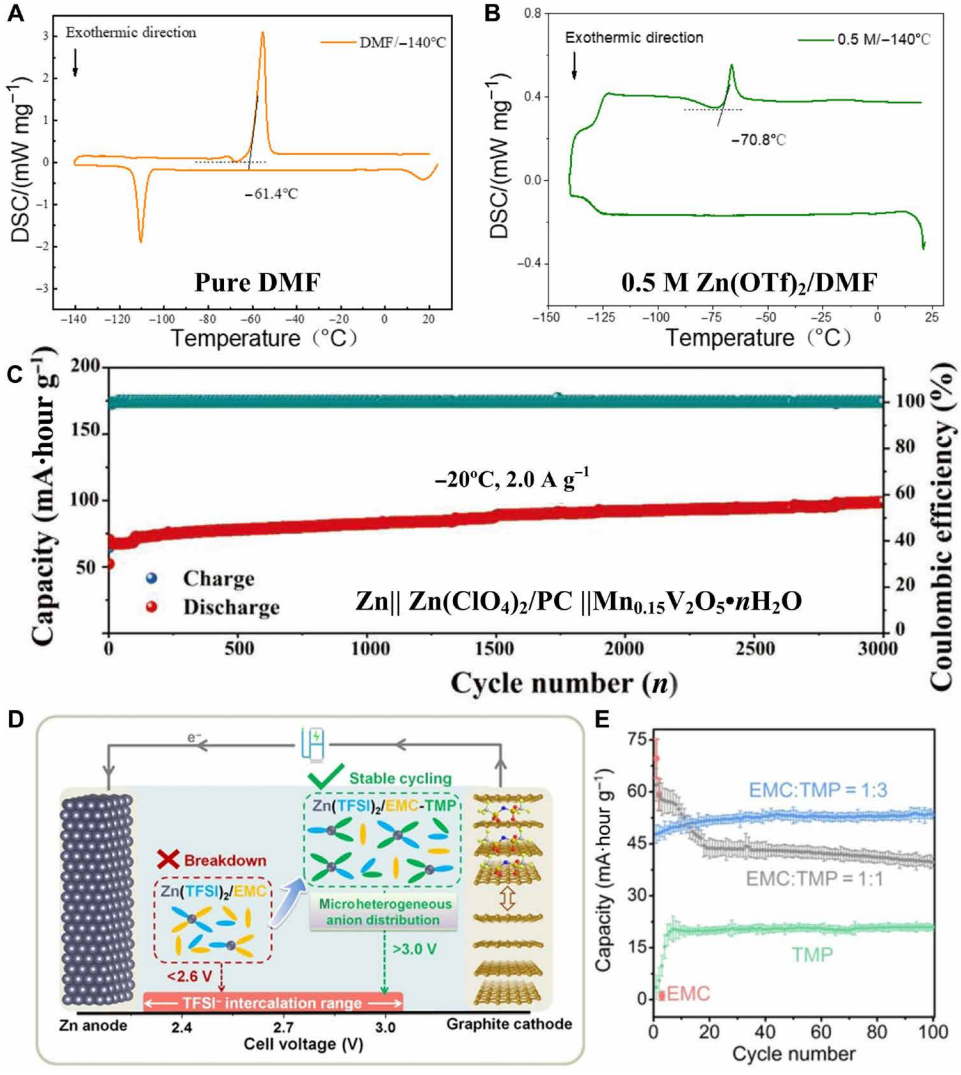

Fig. 5. Recent advances on antifreezing organic solvent–based nonaqueous electrolytes. DSC curves for (**A**) pure DMF and (**B**) 0.5 M $Zn(OTf)_2$/DMF electrolytes down to −140°C. (A) and (B) are reproduced with permission from John Wiley and Sons (*11*). (**C**) Long cycling performance of $Mn_{0.15}V_2O_5{\cdot}nH_2O$ electrode in $Zn(ClO_4)_2$/PC at 2.0 A g^{-1} at −20°C. Reproduced with permission from John Wiley and Sons (*52*). (**D**) Illustration of the EMC-TMP electrolyte with a microheterogeneous anion distribution for Zn/graphite cells. (**E**) Capacity retention for Zn/graphite cells based on different electrolytes. (D) and (E) are reproduced with permission from John Wiley and Sons (*54*).

lattice of SN were weakened. Hydrated eutectic Zn electrolytes were prepared by mixing $Zn(ClO_4)_2{\cdot}6H_2O$ and SN without adding extra water, and an ultralow eutectic temperature of −95.3°C was achieved under the 1:8 of Zn salt/SN molar ratio. Zn||PDB battery, where PDB is poly(2,3-dithiino-1,4-benzoquinone), based on the $Zn(ClO_4)_2{\cdot}6H_2O$/SN electrolyte showed a capacity of 50 mA·hour g^{-1} at −20°C, a capacity retention of 85.4% over 3500 cycles, and almost 100% of Coulombic efficiency (CE) at room temperature (*60*).

In general, organic solvents with the following characteristics can be used to boost the electrochemical performance of ZMBs at subzero temperatures by suppressing T_m of the electrolyte and eliminating water-related parasitic reactions: (i) low melting point and high boiling point, (ii) low viscosity, (iii) relatively high polarity to dissolve ionic salts, (iv) affordability, and (v) wide availability. However, the development of most organic solutions is still challenging because of the low ionic conductivity or the poor solubility of zinc salt with solvents (*11*).

Antifreezing additives/cosolvents for water-based electrolytes

Because of their "small dosage" and "quick effect" properties, considerable attention has been paid to electrolyte additives and cosolvents (*61*). The mechanism of reducing the freezing point of aqueous electrolyte with additive or cosolvent is based on destroying HBs within the water network by the competitive interaction between additives/cosolvents and water molecules. Widely used antifreezing additives or cosolvents include EG (*23*, *27*, *62*, *63*), MeOH (*24*), 1,3-dioxolane (DOL) (*64*), DMSO (*65*–*67*), AN (*68*, *69*), etc.

EG is a typical antifreeze due to its low freezing point and high boiling point (*23*). In addition, characteristics including good solubility in water, a high dielectric constant, a high flash point, and low cost render it a promising electrolyte solvent additive. The freezing point of a mixture of EG and water decreased to −33°C when the EG-to-water volume ratio reached 60% (EG60), as shown in Fig. 6A. The special solvation interaction of Zn^{2+} with EG, which intensifies the HBs between EG and H_2O, broke the HBs between water molecules

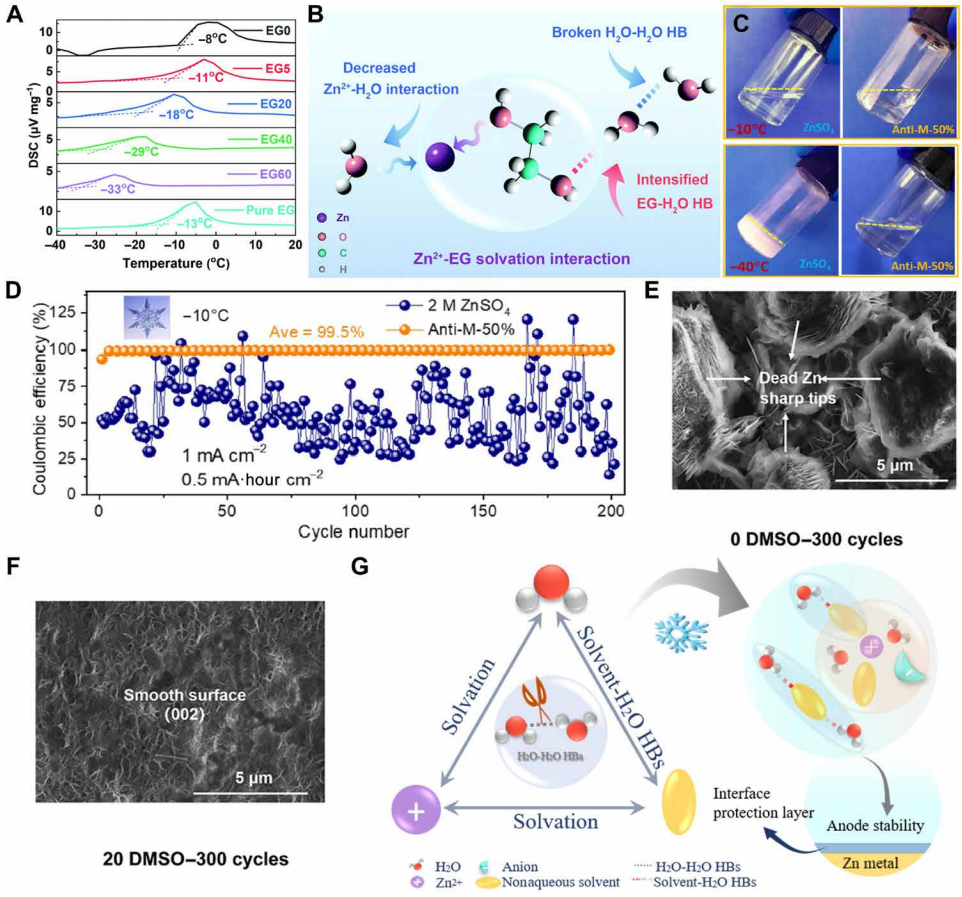

Fig. 6. Recent advances on antifreezing water–based electrolytes with additives/cosolvents and illustration of the main interactions between different electrolyte components that affect the H_2O-H_2O HBs. (**A**) Freezing point data and DSC curves of electrolytes with different EG/H_2O content ratio. (**B**) Schematic illustration of the Zn^{2+}-EG solvation and the chemistry of the hybrid electrolyte. (A) and (B) are reproduced with permission from the Royal Society of Chemistry (*23*). (**C**) Digital photographs of $ZnSO_4$ and anti-M-50% electrolytes at −10° and −40°C. (**D**) Zn reversibility comparison of Zn/Cu cells with $ZnSO_4$ and anti-M-50% electrolytes at −10°C. (C) and (D) are reproduced with permission from John Wiley and Sons (*24*). Scanning electron microscope (SEM) images of Zn anode in Zn/MnO_2 cells with (**E**) 0 DMSO and (**F**) 20 DMSO after 300 cycles at 10°C. (E) and (F) are reproduced with permission from John Wiley and Sons (*65*). (**G**) Illustration of interactions among water molecules, zinc anion, and solvent (solvent additive or cosolvent), and their impact on the electrolyte solvation structure and the stability of the zinc anode.

and weakened the solvation interaction between Zn^{2+} and H_2O, as illustrated in Fig. 6B. ZMBs with 2 M $ZnSO_4$/EG40 electrolyte delivered a high energy density of 121 Wh kg^{-1}, a high power density of 1.7 kW kg^{-1}, and a long-cycle life of 250 cycles at −20°C (*23*). In addition to EG, which belongs to the class of polyhydric alcohols, monohydric alcohols, such as MeOH with a low freezing point of −97.8°C, can be used as antifreezing solvents as well. Anti-M-50% (2 M $ZnSO_4$, H_2O, and 50 volume % MeOH) was designed to boost Zn reversibility and widen the operating temperature of ZMBs. In Fig. 6C, anti-M-50% electrolyte maintained its liquid state, while 2 M $ZnSO_4$ froze as the temperature decreased from −10° to −40°C. Excellent electrochemical performance with an average CE of 99.5% and negligible fluctuations can be observed in Fig. 6D (*24*).

DOL has high ionic conductivity and low viscosity. Its special ring structure completely exposes the lone pair of electrons on its O atom, resulting in the formation of HBs with H_2O. A Zn/V_2O_5 cell based on 1 M $Zn(OTf)_2$/DOL/H_2O exhibited a superior low-temperature performance over 300 cycles at −30°C (*64*).

DMSO is a commonly used solvent because of its high polarity, high boiling point, thermal stability, and its ability to dissolve various inorganic salts (*70*). Dead zinc sharp tips appeared in the electrolyte without DMSO, while a smooth zinc anode surface was obtained after 300 cycles in hybrid electrolyte, as demonstrated in Fig. 6 (E and F), highlighting the capability of DMSO hybrid electrolyte in texturing the Zn metal nucleation on the basal plane (*65*). The interaction between the O atom in the S═O bond of DMSO and the H atom in the O─H bond of a water molecule leads to a stable hydrogen network, and the formation of ice is prevented (*71*). Nian *et al.* (*66*) found that the water/DMSO mixture (molar fraction, $\chi = 0.3$) did not freeze until the temperature was reduced to −130°C, which was much lower than the freezing points of pure DMSO (18.9°C) and pure water (0°C).

It is noteworthy that there are exceptions for some potential additives/cosolvents with H-bonding acceptors. Organic compounds such as ethylene oxide (*72*), tetrahydrofuran (*73*), and 1,4-dioxane (*74*), which can form clathrate hydrates with water molecules,

may not always be able to suppress the freezing point. Although ethylene oxide, tetrahydrofuran, and 1,4-dioxane share similar structures with DOL, they generate totally different effects after being added into water.

To summarize, when designing water-based electrolytes with solvent additives or cosolvents for low-temperature operation, it is necessary to determine the interactions between the zinc ions, solvent, and water, which can have an impact on the H_2O-H_2O HBs (Fig. 6G). An ideal additive/cosolvent for future practical application should not only be able to enhance low-temperature adaptability but also generate a stable Zn^{2+}-conducting interphase to protect the metal anode for long-term cycling. Therefore, the characteristics of additives/cosolvents listed below are noteworthy: (i) low melting point, (ii) miscibility with water, (iii) suitable HB acceptor and donor numbers (DNs), (iv) high ionic conductivity, (v) high electrochemical and thermodynamic stability, and (vi) low cost. Constructing stable HBs between additives/cosolvents and water molecules is the key concept in designing an antifreezing aqueous electrolyte. In the meantime, additional functions and effects of additives or cosolvents, such as forming an SEI layer on the anode and suppressing cathode dissolution, were also found. Some inorganic and organic additives, such as $Zn(H_2PO_4)_2$ (*75*) and dopamine (*76*), have shed light on forming in situ generated SEI layers in water-based electrolytes, by showing good protective effects on the metal anode and a good ability to inhibit dendrites. Therefore, in addition to their temperature adaptability, the additives/cosolvents also deserve a complete work for understanding their influence on both electrodes and for expanding their use.

Antifreezing hydrogel electrolytes

Flexibility and multifunctionality make hydrogel an ideal candidate for fabricating electrolytes for flexible and wearable devices. The inevitable freezing of conventional hydrogels at or near 0°C, however, seriously degrades their electrochemical and mechanical performance and affects practical applications at extremely low temperatures (*77*).

Hydrogels are typically composed of elastic cross-linked hydrated polymer chains with interstitial spaces filled with abundant water (*78*). Water is classified into three different states that are nonbound water (NBW), weakly bound water, and strongly bound water (SBW), according to its interaction with hydrogel (*79*). The intense interaction between NBW and other free water molecules through HBs contributes to the formation of ice, endowing NBW with a high freezing point of 0°C. Considering that the freezing point of SBW is about −100°C, the freezing temperature of hydrogel can be suppressed by two methods: (i) breaking HBs between water molecules by introducing salts or solvents or (ii) intensifying the interaction between water and the hydrogel by modifying the hydrogel network.

Taking advantage of the colligative property of hydrogels and the water-in-salt strategy, adding a salt solution into a hydrogel is a convenient method to decrease the freezing temperature of the hydrogel. The salt concentration, salt type, and compatibility of the salt and the hydrogel are all critical factors. Concentrated KOH solution was added into the double network of a hydrogel composed of poly(2-acrylamido-2-methylpropanesulfonic acid potassium salt) (PAMPS-K) and methyl cellulose (MC), as shown in Fig. 7A. The combination of a concentrated KOH solution and a hydrogel brings an extremely high ionic conductivity of 105 mS cm^{-1} at 25°C (*80*). The Raman spectra in Fig. 7B investigated the structure of water molecules in polyacrylamide (PAAm, also known as PAM) hydrogel, PAM hydrogel with 2 M $ZnSO_4$ (Z-PAM), and PAM hydrogel with 2 M $ZnSO_4$ and 4 M LiCl (ZL-PAM). Reduced intermolecular HBs at 3220 cm^{-1} and intensified asymmetric stretching at 3420 cm^{-1} indicated that more water molecules were bonded to the ions in ZL-PAM. The freezing point of PAM hydrogel was effectively lowered from −15° to −45°C by cooperatively hydrated Zn^{2+} and Li^+ ions, achieving almost 100% of capacity retention and more than 99.5% of CE over 500 cycles at −20°C (*15*).

Introducing organic additives that form HBs with water molecules is also an effective strategy to inhibit ice formation in hydrogels. There are three typical approaches to introducing organic components: (i) gelation in a binary solvent, (ii) solvent displacement, and (iii) chemical cross-linking of hydrogel and organic additives. As a typical antifreeze, EG was introduced into guar gum/sodium alginate (GG/SA) hydrogels via a solvent displacement–induced toughening method. The soaking time and EG volume ratio in the solution were varied to obtain a good balance between the antifreezing property and the ionic conductivity. The GG/SA/EG/metal salt electrolyte yielded a high ionic conductivity of 6.19 mS cm^{-1} at −20°C (*81*). Nonsacrificial HBs between organic molecules and polymer chains are vulnerable to debonding. The stability of hydrogels prepared by the "gelation in binary solvent" or "solvent displacement" methods is not satisfactory in some cases. Decorating the hydrogel with organic solvent through chemical cross-linking is an effective solution. Mo *et al.* (*82*) used EG and isophorone diisocyanate as monomers to synthesize glycol-waterborne anionic polyurethane acrylate and PAM (denoted as EG-waPUA/PAM). An all-round hydrogel was prepared using cotton-derived cellulose, TEOS, and glycerol as the polymeric framework, cross-linker, and antifreezing agent, respectively, and the synthesis process is shown in Fig. 7C. Because of the strong interaction between the hydroxyl groups of glycol and water molecules, the high-salt concentration, and the hydroxyl groups on the cellulose framework, the CT3G30 hydrogel reached an ultralow freezing point of −64.6°C (*19*).

Another effective method to lower the freezing point is to modify the hydrogel with charged/hydrophilic groups that have a strong interaction with water. Leng *et al.* (*83*) fabricated poly(sulfobetaine methacrylate), which is a kind of polyzwitterionic hydrogel electrolyte (PZHE). Charged anionic/cationic groups ensured good adhesion between the electrode and the gel electrolyte, inducing an even ion distribution on the surface of the electrode and a high ion transference number, as shown in Fig. 7D. Density functional theory calculations, as in Fig. 7E, showed that the hydrophilic alkalified carboxyl groups in A-PAA had the highest interaction energy (E_{int}) with water molecules among the four. Thus, HBs among water molecules in A-PAA were the weakest, and the A-PAA had a lower freezing point (−36.8°C), superior flexibility, and high ionic conductivity (199 mS cm^{-1} at −20°C). After being dried for 24 hours, the A-PAA can still remain transparency and presents excellent flexibility at −20°C, as shown in Fig. 7F, further demonstrating its good water retaining capacity and antifreezing properties (*20*).

The design and fabrication of antifreezing hydrogel electrolytes for ZMBs can follow these rules: (i) introducing a concentrated salt solution, (ii) introducing antifreezing organic additives, and (iii) synthesizing or modifying the hydrogel with charged or hydrophilic groups. It should be mentioned that, compared with the liquid electrolyte discussed in "Concentrated aqueous electrolyte," "Organic solvent–based nonaqueous electrolytes," and "Antifreezing additives/cosolvents

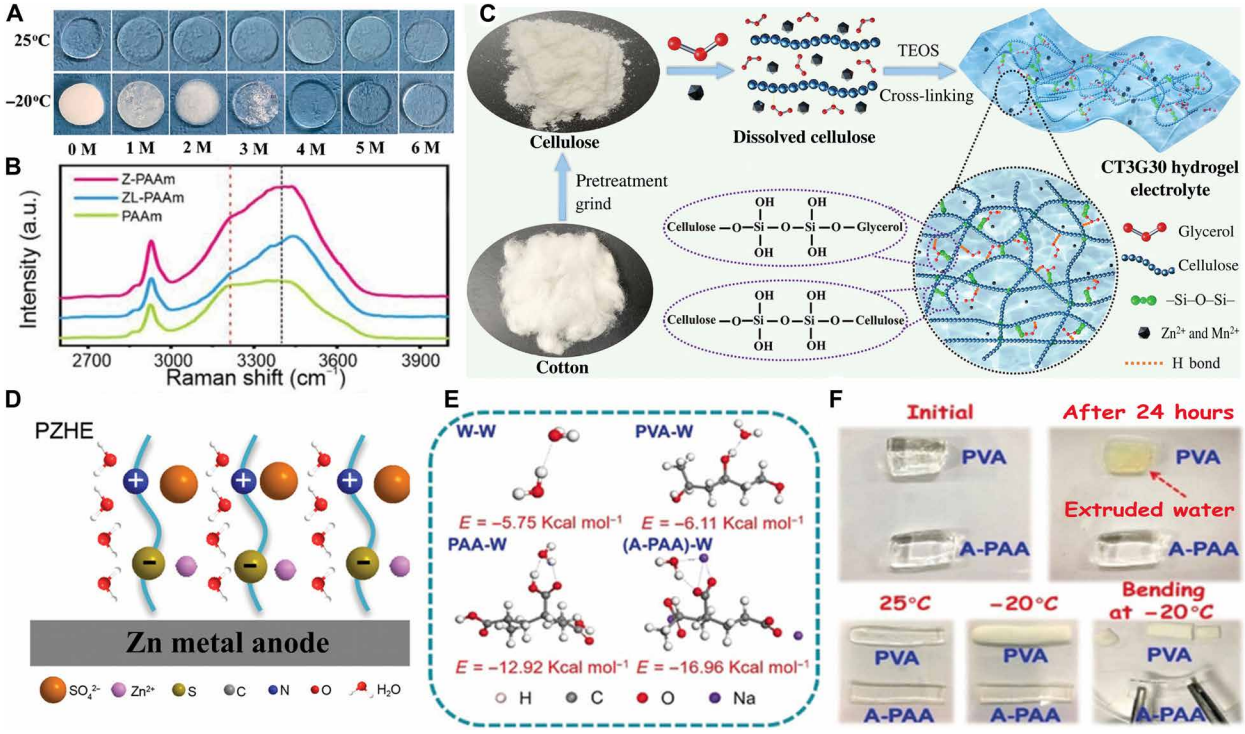

Fig. 7. Recent advances on antifreezing hydrogel electrolytes. (**A**) Digital photographs of PAMPSK25-MC2.0 hydrogels prepared in KOH solutions with different C_{KOH} at 25° and −20°C. Reproduced with permission from the American Chemical Society (*80*). (**B**) Raman spectra of the PAAm, Z-PAAm, and ZL-PAAm in specific ranges. Reproduced with permission from John Wiley and Sons (*15*). (**C**) Schematic illustration of the fabrication of CT3G30 hydrogel electrolyte. Reproduced with permission from John Wiley and Sons (*19*). (**D**) Schematic illustration of the morphology of Zn metal anode with polyzwitterionic hydrogel electrolyte (PZHE) during Zn plating. Reproduced with permission from John Wiley and Sons (*83*). (**E**) Molecular models for simulating interactions between water molecules and various terminal groups in polymers. (**F**) Digital photographs showing a comparison of the water retention and antifreezing properties of A-PAA and polyvinyl alcohol (PVA) hydrogels. (E) and (F) are reproduced with permission from John Wiley and Sons (*20*).

for water-based electrolytes" sections, extra attention needs to be paid to the mechanical properties of quasi-solid hydrogels at subzero temperatures, since hydrogels are always applied in flexible devices.

High-temperature electrolytes

Extreme conditions, such as in a hot desert, require energy storage systems to be reliable, highly efficient, and safe at elevated temperatures. Good volatility and flammability of the solvent in the electrolyte, however, cause swelling and ignition of the battery, inhibiting batteries from working properly.

Volatilization of the electrolyte can be suppressed by two methods: (i) concentrated electrolyte and (ii) the complete/partial replacement of water with solvents with low volatility, such as nonflammable solvents. A Zn-MnO_2 battery based on an oversaturated gel electrolyte can achieve a specific capacity of 301.6 mA·hour g^{-1} at 80°C (*40*). Replacing water with a solvent with a high boiling point is the other way to impair the volatility of electrolyte. As shown in Fig. 8A, Zinc//PQ-MCT batteries with 0.5 M $Zn(OTf)_2$/DMF could operate in a wide temperature range from −70° to 150°C and yielded a capacity of 196 mA·hour g^{-1} at 150°C, which almost doubled that at 25°C (108 mA·hour g^{-1}) (*11*). TEP is a fire-retardant solvent with a high boiling point (215°C), and it favors nonflammability compared to most reported solvents. On the basis of a mixture of PC, TEP, and $Zn(OTf)_2$, a nonflammable organic electrolyte was prepared for a high-voltage Zn//polytriphenylamine battery. The addition of TEP effectively enhanced the nonflammability of the electrolyte in the flammability test in Fig. 8B. The FTIR results in Fig. 8C also reveal that the intimate anion-carbonate (i.e., OTf^--PC) association was decoupled by TEP, leading to a wider electrochemical stability window and better reversibility of the zinc anode (*55*). Liu *et al.* (*6*) proposed 0.5 M-$Zn(OTf)_2$/TEP:H_2O as a hybrid electrolyte to lift the battery's upper safe operating temperature. Water-related parasitic reactions were also suppressed, because the interaction between Zn^{2+} ions and TEP is the strongest compared to the interacting force in Zn^{2+}-OTf^- and Zn^{2+}-H_2O (Fig. 8D), and the inner solvation sheath of Zn^{2+} is occupied by TEP (Fig. 8E). Ionic liquids with intrinsic low flammability and negligible volatility, such as acetamide/zinc perchlorate hexahydrate with PAM, can be used to synthesize electrolytes with good thermal stability (*84*).

Hydrogels can also be used for high-temperature applications if water can be retained in the hydrogel structure. To have good water retention ability, hydrogels should have these characteristics: (i) chemical groups that can interact with water molecules and (ii) a coating layer that can avoid the escape of water. A supramolecular-polymer double-network (SP-DN) hydrogel with guanosine-cyclohexylboronic acid (G-CyBA) and PAM was prepared by using a one-pot method, as shown in Fig. 8F. Because of multiple interactions, ionic conductivity of the KOH (6 M)–filled SP-DN hydrogel electrolyte reached 431.7 and 3.2 mS cm^{-1} at 100° and −80°C, respectively, as demonstrated in Fig. 8G (*85*). Inspired by the phenomenon that epidermis

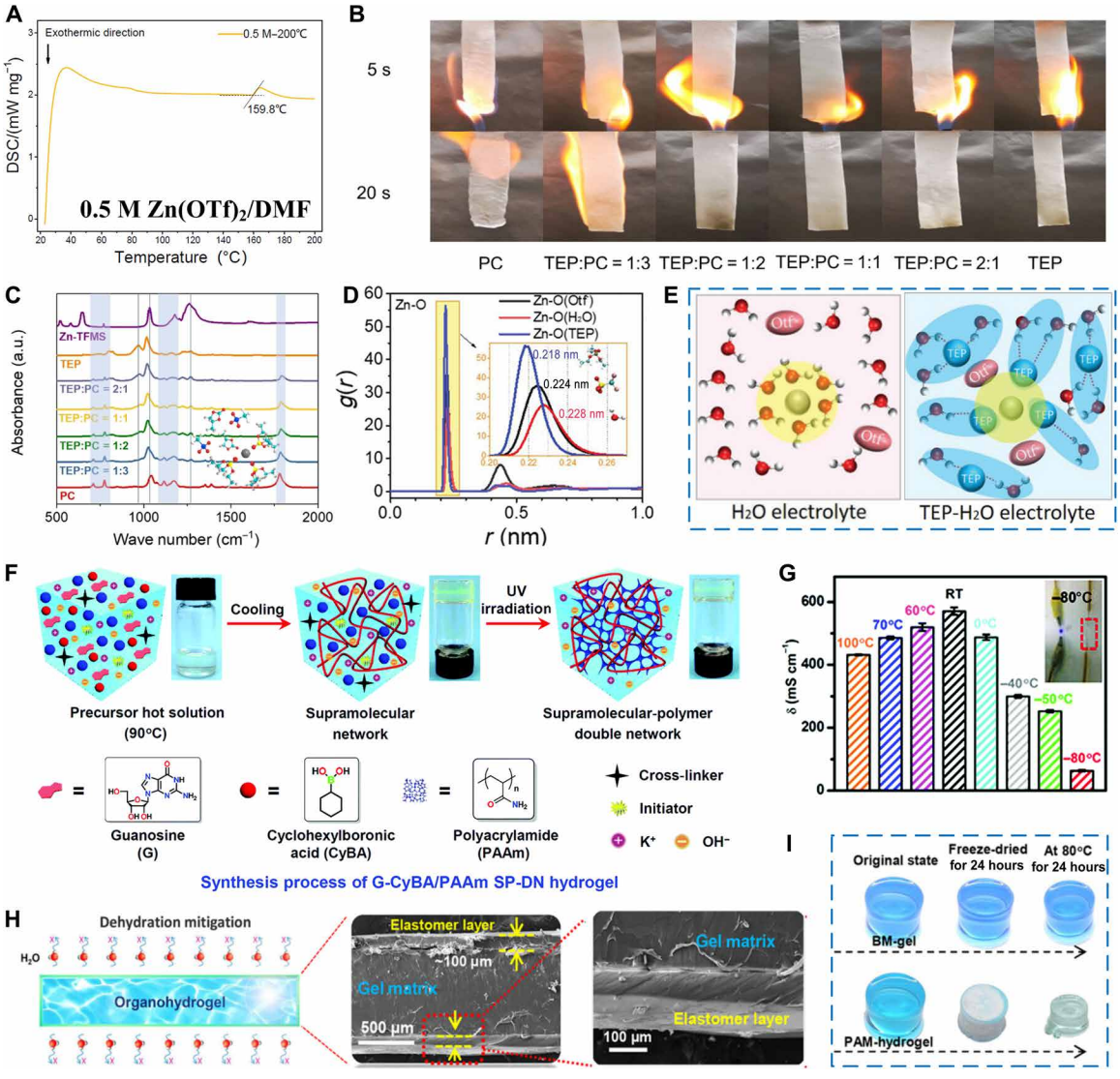

Fig. 8. Recent advances on electrolytes for high-temperature operation. (**A**) DSC curve for 0.5 M $Zn(OTf)_2$/DMF electrolyte heated up to 200°C. Reproduced with permission from John Wiley and Sons (*11*). (**B**) Flammability test for electrolytes. (**C**) FTIR spectra of different $Zn(OTf)_2$/ (TEP/PC) electrolytes. (B) and (C) are reproduced with permission from John Wiley and Sons (*55*). (**D**) Calculated radius distribution of O atoms from H_2O, OTf^-, and TEP molecules around Zn^{2+} for the electrolyte with a TEP volume ratio of 50%. (**E**) Illustration of the Zn^{2+} centered solvation structures for pure aqueous electrolyte and $Zn(OTf)_2$-TEP-H_2O electrolyte. (D) and (E) are reproduced with permission from John Wiley and Sons (*6*). (**F**) Illustration of the synthesis process for G-CyBA/PAAm SP-DN hydrogel. UV, ultraviolet. (**G**) Conductivity of 600% KOH (6 M)–filled G-CyBA/PAAm SP-DN hydrogel at different temperatures. RT, room temperature. (F) and (G) are reproduced with permission from the Royal Society of Chemistry (*85*). (**H**) Illustration and SEM image of BM-gel electrolyte. (**I**) Digital photographs of BM-gel and PAM-hydrogel electrolytes after being heated to 80°C or freeze-dried for 24 hours. (H) and (I) are reproduced with permission under the terms in https://creativecommons.org/licenses/by/4.0/ (*86*).

covers the muscle tissue to prevent dehydration, an elastomer layer was chemically coated on the surface of a hydrogel to form a biomimetic organohydrogel (BM-gel) electrolyte and avoid migration of water molecules from inner gel matrix to the external environment (Fig. 8, H and I). The ingenious design of the elastomer greatly improved the wide temperature range operability of the battery, delivering a capacity of 105 mA·hour g^{-1} at a current density of 2 A g^{-1} under 80°C and 165 mA·hour g^{-1} at a current density of 0.2 A g^{-1} under −20°C, respectively (*86*).

The high temperature will result in electrolyte oxidation, which leads to electrolyte consumption through chemical or electrochemical reactions. These reactions may be accelerated when the cathode contains transition metal elements, which may have catalytic effects (*29*). In addition, an organic cathode is likely to dissolve in organic solvent–based electrolytes, and some inorganic cathodes can dissolve or decompose at high temperatures (*11*, *29*, *87*). Thus, the influence of the cathode on the electrolyte should be considered when designing suitable electrolytes or evaluating the battery performance at high temperatures.

In conclusion, the design of ZMBs with wide temperature operability and high safety can be based on the following principles: (i) highly concentrated electrolyte, (ii) solvents with poor volatility, (iii) hydrogel with hydrophilic or charged groups, and (iv) hydrogel with coating for maintaining moisture. When it comes to practical

application, other than volatility and flammability, more properties such as cost, and biological and environmental toxicity need to be taken into consideration (*86*).

SUMMARY AND OUTLOOK

Summary of different electrolyte strategies

The electrochemical performance of ZMBs is challenged by extreme temperature applications due to the freezing or volatility of electrolytes. Several approaches are adopted to prepare electrolyte for low- and high-temperature usage, and these types of electrolytes show different merits from the aspects of the working temperature range, ionic conductivity, viscosity, cost, chemical stability, or thermal stability, as rated and compared in Fig. 9A. To be specific, compared with the innovative strategies, the traditional aqueous electrolytes that normally have a dilute concentration, such as 0.5 M $ZnSO_4$, have innate advantages in terms of high ionic conductivity, low viscosity, and low cost. The WIS strategy can broaden the operating temperature, expand the electrochemical stability window, alleviate the dissolution of the cathode and corrosion of the anode, and increase the metal ion transference number. It also has disadvantages, however, such as high viscosity, crystal precipitation, high salt cost, and the huge quantity used in WIS electrolyte. Most of the reported concentrated electrolytes use either low-cost $ZnCl_2$ or other rare salts, which all sacrifice viscosity and some ionic conductivity. The hybrid electrolyte with cosolvent may share some similar advantages to all organic solvent–based electrolytes with respect to chemical and thermal properties, but it is also highly dependent on the ratio and intrinsic properties of the cosolvent in the aqueous solution. Some excellent organic solvents with low T_m can boost the electrochemical performance of ZMBs at subzero temperatures by suppressing the T_m of the electrolyte and eliminating parasitic reactions. Although in the case of most of the reported organic solvents, their intrinsic flammability and low ionic conductivity may hinder their application, some of them can be used as cosolvents to overcome this shortcoming and enable a suitable SEI by mixing with the aqueous solution. The antifreezing additives are used to construct stable HBs between the additives and the water molecules but usually do not have an apparent influence on the overall properties of the original electrolyte. The antifreezing property of a hydrogel can be improved using the same solutions as for a water-based electrolyte, increasing the salt concentration, adding antifreezing additives/cosolvents.

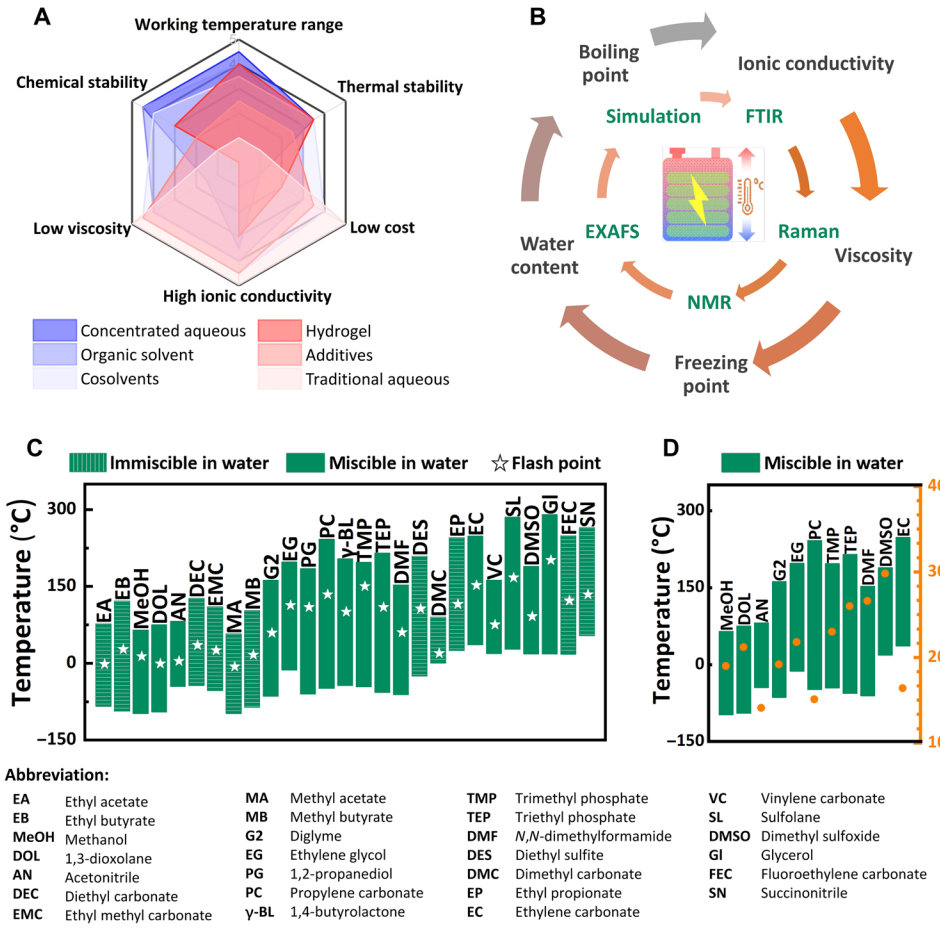

Fig. 9. Comparison of different electrolyte design strategies and potential candidates as solvents or additives/cosolvents for ZMBs that can operate at harsh temperatures. (**A**) Spider chart for an itemized comparison of different types of electrolytes in ZMBs based on their summarized performances. (**B**) The key parameters and in-depth analysis techniques for the study of electrolytes intended for harsh temperature applications. (**C**) Liquid temperature range, miscibility in water, and flash point of organic solvents that are promising to use in ZMBs for harsh temperature application. (**D**) Liquid temperature range and DN of water-miscible organic solvents that are promising candidates as additives/cosolvents for ZMBs operating at harsh temperatures.

Therefore, apart from the viscosity and cost, most hydrogel electrolytes can approach high ionic conductivity and thermal stability that are as good as for the water-based electrolytes. Synthesis or modification of a hydrogel with charged or hydrophilic groups can achieve excellent low-temperature performance as well.

In assessing the full battery performance, most reports used superfast testing current rates on cathode materials, presenting excellent capacities but ignoring the proton cointercalation or side reactions between the materials and the electrolyte. In addition, most of the electrolytes reported to work under extreme conditions were tested at a selected temperature, without investigating more physical properties, such as the thermal stability range of the electrolyte.

Specifically, all the electrolytes are generally recommended to have high ionic conductivity, a low freezing point, low viscosity, low free water content, and low flammability (see Fig. 9B) for beyond-room-temperature utilization. Besides these physical properties, in-depth probing of the electrolyte structure is important for further understanding its interfacial behavior on electrodes. The coordination environment of different electrolyte components can preliminarily be analyzed via spectroscopy techniques (Raman and FTIR) via shifts in the wave number and intensity changes of the chemical functional groups. Precise analysis of the complex structure of an electrolyte requires advanced nuclear magnetic resonance or synchrotron-radiation extended x-ray absorption fine structure, which, however, has limitations on the elements that can be characterized or is distant from most battery researchers. The computing simulation method is one of the most effective ways for acquiring detailed information about the electrolyte structure and predicting the possible interfacial reactions.

On the basis of the above discussions on the reported strategies and key parameters, a selection pool of the promising additives/solvents for different temperature ranges has been composed. Figure 9C shows the potential organic additives/solvents, which could be selected for application at different temperatures according to their intrinsically stable liquid window. In the real situation, however, the temperature stability window of the electrolyte may differ from the intrinsic property of the solvent, since the interaction of different electrolyte components can affect the freezing or evaporation performance of the whole solution. For additives/solvents in water-based electrolytes, the Gutmann DN is critical for determining the bonding strength with H_2O, which is important for reducing the water activity. A solvent that has a higher DN than H_2O (DN = 18 kcal mol^{-1}) could be a good candidate to be used in a small dosage but can lead to a good effect in forming HBs and thus enhance the temperature adaptability. In this respect, Fig. 9D lists some water miscible solvents for extreme temperature use and compares the DN values of these solvents. According to the DN value, MeOH, DOL, diglyme (G2), EG, TMP, TEP, DMSO, and DMF are good candidates as additives/cosolvents for manipulating the HBs between water molecules.

Road to practical application

After intensive development, ZMBs have been broadly studied to address the scientific issues relating to both cathode and anode as well as the electrolyte with publications. The future commercialization of ZMBs for grid scale and other stationary energy storage requires variable temperature operation, which is highly reliant on the joint improvements on energy density, cycle life, and harsh temperature adaptability.

In view of the above status, the further development of ZMBs for harsh environment deployment needs to take the industrial requirements into account in their early-stage consideration. The recent studies on extending the working temperatures for ZMBs have highlighted several promising methods, through adjusting the concentration, introducing additives, adopting water-organic solvents hybrid strategy, using all-organic solvents, or using various sol-gel approaches. As summarized in Fig. 3 and Table 1, the Mn- and V-based cathodes, such as MnO_2, $Mg_xV_2O_5$, and $VOPO_4$, exhibit great prospects for high capacity and relatively high operational voltage at various temperatures. Besides high energy density, the actual requirements for grid-scale application of ZMBs are safety and low cost. Thus, aqueous electrolytes and their derivative hybrid electrolytes with additives or organic solvents are most likely to offer these advantages along with practical pathways to ZMB technology. Although the separator does not directly participate in electrochemical reaction in ZMBs, its properties such as porosity, pore size, permeability, chemical/physical stability, ionic conductivity, dimensional stability, mechanical strength, and thermal shrinkage will have a great impact on the overall performance of the batteries in terms of their cycling performance, safety, internal resistance, and capacity. For application under harsh temperature conditions, the chemical/physical stability and thermal shrinkage are two factors that require extra attentions. The permeability, wettability, and ability of the separator to take up and retain electrolyte will affect the dendrite growth of the Zn anode. Separators with high permeability will facilitate a more uniform ionic flow. Good ability of the separator to take up and retain electrolyte will contribute to an uninterrupted supply of ionic flux and a lower concentration gradient. Thus, the dendrite growth will be suppressed (*35*).

The current industrial processes for ZMBs are in their infancy, due to the currently inferior performance of these batteries under practical testing protocols, which refer to using industrial testing methods under harsh environments. Although there are various innovations aimed at improving the overall performance of ZMBs, the major achievements are limited to bench-scale tests. The future energy density goal for ZMBs should be over 90 Wh kg^{-1}, while the calculated energy density (based on all battery components) for laboratory research is usually between 50 and 80Wh kg^{-1}, which is still below industrial needs (*88*). Specifically, the bench research is usually optimized while neglecting other factors, such as the cathode loading, the electrolyte amount, metal anode thickness, safety, and cost, which is inadequate for practical applications. Although it might be too early to require the development of specific practical testing protocols for ZMB electrolytes, the current fundamental studies on electrolytes should at least emphasize these directions: (i) the working temperature range, (ii) the working voltage window, (iii) the compatibility with the cathode material and zinc metal anode, and (iv) the safety considerations and dosage for their matched cathode/anode.

To sum up, the rapid evolution of ZMBs is calling for systematic research to cope with external environmental changes for practical deployment. Although LIBs will still dominate the energy storage market in the next decade, the bright future of ZMBs toward deployment as grid energy storage will continually encourage their forefront study and will advance their progress toward commercialization. Therefore, improving the output energy density of ZMBs to suit the demand for beyond-room-temperature application is an urgent necessity. There have been tremendous efforts on optimizing the

Table 1. Summary of different types of electrolytes for operating at harsh temperatures. The physical parameters and full cell performance of four categories of electrolytes in ZMBs that were applied above or below room temperature. The symbol "*" represents there is no related data not provided in the cited work.

Category	Electrolyte	Ionic conductivity (mS cm^{-1})	Freezing point (°C)	Operating temperature range (°C)	Cathode	Capacity of the full cell			Ref.
						Capacity	Current density	T (°C)	
Concentrated aqueous electrolyte	7.5 M $ZnCl_2$/H_2O	1.79 (−60°C)	−114	−90–+60	PANI	50.6 mA·hour g^{-1}	0.01 A g^{-1}	−90	(*1*)
	7.6 m $ZnCl_2$/0.05 m $SnCl_2$/H_2O	0.8 (−70°C)	*	−70–+20	$VOPO_4$	48.7 mA·hour g^{-1}	1/3 C	−70	(*89*)
						163 mA·hour g^{-1}		20	
	4 M $Zn(BF_4)_2$/H_2O	1.47 (−70°C)	−122	−95–+25	TCBQ	63.5 mA·hour g^{-1}	0.22 A g^{-1}	−95	(*16*)
						101.4 mA·hour g^{-1}		−30	
	2 M $Zn(OTf)_2$/H_2O	4.47 (−30°C)	−34.1	−30–+25	V_2O_5	285 mA·hour g^{-1}	0.1 A g^{-1}	−30	(*35*)
	3 M $Zn(OTf)_2$/H_2O	*	*	−10–+50	V_2O_5	470 mA·hour g^{-1}	0.2 A g^{-1}	RT	(*13*)
	3 M $Zn(OTf)_2$/H_2O	*	*	−20–RT	$(NH_4)_2V_6O_{16}·1.5H_2O$	41 mA·hour g^{-1}	1 A g^{-1}	−20	(*90*)
						280 mA·hour g^{-1}		RT	
	3 M $Zn(OTf)_2$/H_2O	6.716 (−30°C)	<−60	−30–+25	$NH_4V_4O_{10-x}·nH_2O$	329.3 mA·hour g^{-1}	0.1 A g^{-1}	−30	(*91*)
						484.3 mA·hour g^{-1}		25	
	3 M $Zn(OTf)_2$/H_2O	*	*	−20–+20	$K_{0.5}V_2O_5$	162 mA·hour g^{-1}	5 A g^{-1}	−20	(*92*)
						256 mA·hour g^{-1}		20	
	3 M $Zn(OTf)_2$/H_2O	*	*	0–+50	Zinc foil				(*93*)
	4 M $Zn(TFSI)_2$/H_2O	90	−38	−35–+25	$P(4VC_{86}$ - stat -$SS_{14})$	179 mA·hour g^{-1}	688 mA g^{-1}	−35	(*17*)
						213 mA·hour g^{-1}		−25	
						325 mA·hour g^{-1}		25	
	2 M $ZnSO_4$/H_2O	*	*	0–+50	$NH_4V_4O_{10}$	179 mA·hour g^{-1}	5 A g^{-1}	0	(*14*)
						361.6 mA·hour g^{-1}	1 A g^{-1}	25	
						377 mA·hour g^{-1}	5 A g^{-1}	50	
	2 M $ZnSO_4$/H_2O	*	*	0–+50	M-V_2O_5 (M=Fe^{2+},Co^{2+},Ni^{2+},Mn^{2+},Zn^{2+},Cu^{2+})	320 mA·hour g^{-1}	0.5 A g^{-1}	0	(*15*)
						410 mA·hour g^{-1}		50	

continued on next page

Category	Electrolyte	Ionic conductivity (mS cm^{-1})	Freezing point (°C)	Operating temperature range (°C)	Cathode	Capacity of the full cell			Ref.
						Capacity	Current density	T (°C)	
	3 M LiCl/4 M $ZnCl_2/H_2O$	*	*	−10–+50	$LiFePO_4$	93.8 mA·hour g^{-1}	102 mA g^{-1}	−10	(*94*)
						138.3 mA·hour g^{-1}		25	
						148.5 mA·hour g^{-1}		50	
	1 M $Zn(ClO_4)_2/H_2O$	*	*	−20–RT	$V_2O_5{\cdot}nH_2O$/CNT	221 mA·hour g^{-1}	2 A g^{-1}	RT	(*95*)
	3.5 M $Mg(ClO_4)_2$/ 1 M $Zn(ClO_4)_2/H_2O$	1.41 (−70°C)	−121	−70–+25	pyrene-4,5,9,10-tetraone (PTO)	101.5 mA·hour g^{-1}	0.2 A g^{-1}	−70	(*4*)
	6.0 M CsOH/0.20 M $Zn(OAc)_2/H_2O$	*	<−44	−20–+20	Pt/C + Ir/C	99.3 mW cm^{-2}	5.0 mA cm^{-2}	−10	(*45*)
	45 m $ZnBr_{0.5}Cl_{1.5}$/1 m $Zn(OAc)_2/H_2O$	1.28	<−80	−80–+40	PGA	605.7 mA·hour g^{-1}	1 A g^{-1}	25	(*39*)
Organic solvent–based nonaqueous electrolyte	0.5 M $Zn(OTf)_2$/ DMF	18.9 (25°C)	−70.8	−70–+150	PQ-MCT	31.3 mA·hour g^{-1}	0.2 A g^{-1}	−70	(*11*)
						108 mA·hour g^{-1}	2 A g^{-1}	25	
						196 mA·hour g^{-1}		150	
	1.2 M $Zn(TFSI)_2$/ AN	*	*	−40–+80	Graphite	52.2 mA·hour g^{-1}	0.52 A g^{-1}	RT	(*22*)
	$Zn(ClO_4)_2$/ SN(1:8)	5.52	−95.3	−20–+25	PDB	50 mA·hour g^{-1}	48 mA g^{-1}	−20	(*60*)
						95 mA·hour g^{-1}		25	
	1 M $Zn(ClO_4)_2$/ PC	*	*	−20–RT	$Mn_{0.15}V_2O_5{\cdot}n\ H_2O$	190 mA·hour g^{-1}	0.1 A g^{-1}	−20	(*52*)
						367 mA·hour g^{-1}		RT	
	1 M $Zn(ClO_4)_2$/ PC	*	*	−20–RT	$FeVO_4$	240 mA·hour g^{-1}	0.1 A g^{-1}	RT	(*51*)
	1 M $Zn(ClO_4)_2$/ PC	*	*	−20–+25	PEG/V_2O_5	430 mA·hour g^{-1}	0.1 A g^{-1}	25	(*53*)
	4m $Zn(BF_4)_2{\cdot}4.5H_2O$/ EG	4.5	<−80	−30–+40	V_2O_5	5 mA·hour cm^{-2}	0.5 mA cm^{-2}	RT	(*96*)
	$Zn(ClO_4)_2{\cdot}6H_2O$/ SL (1:6)	2	<−80	−40–+20	PANI	76 mA·hour g^{-1}	0.1 A g^{-1}	−40	(*97*)
						160 mA·hour g^{-1}		20	

continued on next page

Category	Electrolyte	Ionic conductivity (mS cm^{-1})	Freezing point (°C)	Operating temperature range (°C)	Cathode	Capacity of the full cell			Ref.
						Capacity	Current density	T (°C)	
Water-based electrolyte with antifreezing additive/ cosolvent	2 M $ZnSO_4$/40 volume % EG/ H_2O	6.9 (−40°C)	*	−40–+20	$PANIV_2O_5$	180 mA·hour g^{-1}	0.1 A g^{-1}	20	(*23*)
	2 M $ZnSO_4$/50% EG/H_2O	*	−43.2	−40–+80	PQ-MCT	20 mA·hour g^{-1}	0.2 A g^{-1}	−40	(*27*)
						63 mA·hour g^{-1}		25	
						152 mA·hour g^{-1}		80	
	3 M $ZnSO_4$/68 volume % EG/ H_2O	*	<−50	−20–+25	$Zn_xV_2O_5{\cdot}nH_2O$	329 mA·hour g^{-1}	0.5 A g^{-1}	25	(*62*)
	1% Et_2O/30% EG/2 M $ZnSO_4$/0.2 M $MnSO_4$/H_2O	420 (−10°C)	*	−10–+25	CNT/MnO_2	90.3 mA·hour g^{-1}	3 A g^{-1}	25	(*63*)
						65.1 mA·hour g^{-1}		−10	
	3 M $ZnSO_4$/20% 1,2-propanediol (PG)/ H_2O	*	−29	−20–+25	V_2O_5	359 mA·hour g^{-1}	0.5 A g^{-1}	25	(*98*)
						190 mA·hour g^{-1}		−20	
	2 M $ZnSO_4$/20 volume % DMSO / H_2O	1.98 (−20°C)	−34.51	−20–+20	MnO_2	170 mA·hour g^{-1}	10 C	20	(*65*)
	2 M $ZnSO_4$/50 volume % MeOH/ H_2O	16.8 (25°C)	−46	−20–+60	PANI	186.3 mA·hour g^{-1}	0.1 A g^{-1}	−10	(*24*)
						219.1 mA·hour g^{-1}		25	
						249.7 mA·hour g^{-1}		60	
	0.5 M-$Zn(OTf)_2$/ 50 volume % TEP/H_2O	*	*	−20–+50	V_2O_5	310 mA·hour g^{-1}	0.1 A g^{-1}	RT	(*6*)
	1 M $Zn(OTf)_2$/50% DOL/H_2O	30	−51.2	−30–RT	$V_2O_5{\cdot}1.6H_2O$	131 mA·hour g^{-1}	0.1 A g^{-1}	−30	(*64*)
	1 M $Zn(OTf)_2$/ 72 volume % AN/ 28 volume % H_2O	28.6 (−40°C)	−55.3	−40–+25	V_2O_5	114 mA·hour g^{-1}	0.05 A g^{-1}	−40	(*99*)

continued on next page

Category	Electrolyte	Ionic conductivity (mS cm^{-1})	Freezing point (°C)	Operating temperature range (°C)	Cathode	Capacity of the full cell			Ref.
						Capacity	Current density	T (°C)	
Antifreezing hydrogel electrolyte	1 m $Zn(OAc)_2$/40 m KOAc/PAA	3.74 (RT), 65.9 (80°C)	*	RT–+80	MnO_2	311.7 mA·hour g^{-1}	1C	RT	(*40*)
	2 M $Zn(OTf)_2$/H_2O/PVA	*	*	0–+100	VO_2 (B)-MWCNTs	230.4 μA·hour cm^{-2}	1.43 mA cm^{-2}	50	(*100*)
	3 M $Zn(OTf)_2$ / H_2O/PAM	1.9 (−30°C)	*	−30–+80	$Mg_{0.1}V_2O_5$ H_2O	272 mA·hour g^{-1}	0.2 A g^{-1}	−30	(*18*)
						459 mA·hour g^{-1}		RT	
						501 mA·hour g^{-1}		80	
	3 M $Zn(OTf)_2$/ H_2O/ PAM/ CNF	10.9 (RT)	*	−18–+40	$H_2V_3O_8$/Mxene	152.5 mA·hour g^{-1}	0.5 A g^{-1}	−18	(*101*)
						307.3 mA·hour g^{-1}		40	
	$ZnCl_2$/$MnSO_4$/ LiCl/PVA	*	*	−20–+100	COG@MnO_2	6.9 mA·hour cm^{-3}	60 mA cm^{-3}	−20	(*102*)
						10.3 mA·hour cm^{-3}		25	
						13.5 mA·hour cm^{-3}		100	
	2 M $ZnSO_4$/0.1 M $MnSO_4$/H_2O/ PVA	*	*	0–+40	δ-MnO_2	219.58 mA·hour g^{-1}	1.5 mA cm^{-3}	RT	(*103*)
	2 M $ZnSO_4$/4 M LiCl/H_2O/PAM	*	−45	−20–+25	$LiFePO_4$	104 mA·hour g^{-1}	0.1 A g^{-1}	−20	(*15*)
						106 mA·hour g^{-1}		25	
	21 M LiTFSI/1 M $Zn(OTf)_2$/H_2O/ PAM	9.1 (25°C), 1.5 (−15°C)	<−23	−15–+25	V_2O_5·nH_2O shell/ V_3O_7·H_2O core	60 mA·hour g^{-1}	0.5 A g^{-1}	−15	(*104*)
						455 mA·hour g^{-1}	0.1 A g^{-1}	25	
	20 M LiTFSI/1 M $Zn(TFSI)_2$/H_2O/ PAM	4.5 (25°C)	<−41	−25–+25	$Co_{0.247}V_2O_5$·0.944H_2O/CFC	432 mA·hour g^{-1}	0.1 A g^{-1}	25	(*105*)
						225 mA·hour g^{-1}		−25	
	21 M LiTFSI/3 M $Zn(OTf)_2$/H_2O/ PVA	2.1 (20°C)	*	0–+40	V_2O_5/GO	325 mA·hour g^{-1}	20 mA g^{-1}	0	(*106*)
						416 mA·hour g^{-1}		40	
	1.5 m $Zn(OTf)_2$/3 m LiTFSI/ H_2O/ BC/PEG	1.20 (−20°C)	−97.6	−20–+25	$LiFePO_4$	49.3 mA·hour g^{-1}	85.3 mA g^{-1}	−20	(*107*)

continued on next page

Category	Electrolyte	Ionic conductivity (mS cm^{-1})	Freezing point (°C)	Operating temperature range (°C)	Cathode	Capacity of the full cell			Ref.
						Capacity	Current density	T (°C)	
	20 M $ZnCl_2$/ H_2O/xanthan gum	13.8 (20°C), 5.0 (−20°C)	*	−20–+20	$NH_4V_3O_8$· 1.9H_2O	119 mA·hour g^{-1}	0.2 A g^{-1}	−20	(*108*)
						215 mA·hour g^{-1}		0	
						283 mA·hour g^{-1}		20	
	4 m $ZnCl_2$/ H_2O/xanthan gum	6.26 (20°C), 2.54 (−20°C)	<−50	−40–+20	$NH_4V_3O_8$•1.9H_2O	83 mA·hour g^{-1}	0.2 A g^{-1}	−40	(*109*)
						201 mA·hour g^{-1}		−20	
						426 mA·hour g^{-1}		20	
	3 M $ZnCl_2$/ H_2O/Pam	9.93 (−20°C), 15.4 (0°C), 16.9 (RT)	−41.14	−20–+20	PANI	0.616 mA·hour cm^{-2}	0.2 mA cm^{-2}	−20	(*110*)
						1.148 mA·hour cm^{-2}		20	
	15 m $ZnCl_2$ / H_2O /CMC	10.08 (RT)	*	0–+60	$K_{0.486}V_2O_5$	339 mA·hour g^{-1}	50 mA g^{-1}	RT	(*111*)
	6 M KOH/0.2 M $Zn(Ac)_2$/H_2O/ PANa	5.7 (−20°C), 12.6 (24°C), 16.3 (50°C)	<−50	−20–+50	NiCo@CC	137 mA·hour g^{-1}	825.6 mA g^{-1}	50	(*112*)
						108 mA·hour g^{-1}	490.2 mA g^{-1}	−20	
	5 M KOH/H_2O/ PAMPS-K/MC	18.1 (−20°C)	−30.5	−20–+25	Co_3O_4/CC	754.2 mA·hour g^{-1}	1 mA cm^{-2}	−20	(*80*)
						758.5 mA·hour g^{-1}		0	
						764.7 mA·hour g^{-1}		25	
	6 M KOH/2 M KI/H_2O/ PAM-CNF	223 (20°C), 110 (−40°C)	−63.3	−40–+20	Pt/RuO_2/CC	743 mA·hour g^{-1}	2 mA cm^{-2}	−40	(*113*)
						818 mA·hour g^{-1}		20	
	3 M $Zn(OTf)_2$/ H_2O/ glycerol/ PVA	10.7(−30°C)	<−30	−30–+60	$Mg_{0.19}V_2O_5$·0.99H_2O	256.3 mA·hour g^{-1}	0.1 A g^{-1}	−30	(*114*)
						445.9 mA·hour g^{-1}		25	
						490.2 mA·hour g^{-1}		60	
	6 M KOH /0.2 M $Zn(Ac)_2$/ H_2O/glycerol/ PAM/PAA	*	*	−20–+70	Pt/C/RuO_2/CC	506.17 mA·hour g^{-1}	1 mA cm^{-2}	−20	(*115*)
						663.25 mA·hour g^{-1}		25	
						640.92 mA·hour g^{-1}		70	
	1 M $ZnCl_2$/0.5 M NH_4Cl/50 wt % EG/PVA	2.89 (−30°C)	<−30	−30–+20	PANI	58.8 mA·hour g^{-1}	1 A g^{-1}	−30	(*116*)

continued on next page

Category	Electrolyte	Ionic conductivity (mS cm^{-1})	Freezing point (°C)	Operating temperature range (°C)	Cathode	Capacity of the full cell			Ref.
						Capacity	Current density	T (°C)	
	2 M $ZnSO_4$/0.2 M $MnSO_4$/GO/EG/PAM	14.9 (−20°C)	*	−20–+20	δ-MnO_2	183.2 mA·hour g^{-1}	0.2 A g^{-1}	−20	(*117*)
						284.8 mA·hour g^{-1}		20	
	2 M $ZnSO_4$/0.1 M $MnSO_4$/EG/GG/SA	6.19 (−20°C)	*	−20–+25	MnO_2	113.8 mA·hour g^{-1}	0.1 A g^{-1}	−20	(*81*)
						274.2 mA·hour g^{-1}		25	
	2 M $ZnCl_2$/3 M NH_4Cl/EG/10% H_2O/PAMPS/PAM	1.62 (−30°C)	<−50	−30–+80	PANI	59.7 mA·hour g^{-1}	0.2 A g^{-1}	−30	(*118*)
	2 M $Zn(OTf)_2$/EG/H_2O/PAM(AF-SH-CPAM)	*	<−50	−20–RT	Au-CNT/ PANI	233.9 mA·hour g^{-1}	0.1 A g^{-1}	RT	(*119*)
						160.3 mA·hour g^{-1}		−20	
	2 M $ZnSO_4$/0.2 M $MnSO_4$/glycerol/cellulose/TEOS(CT3G30)	19.4 (−40°C)	−64.6	−40–+60	rGO/MnO_2	211.9 mA·hour g^{-1}	0.2 A g^{-1}	−40	(*19*)
						277.3 mA·hour g^{-1}		20	
	5 M KOH/20 volume % DMSO/H_2O/PAMPS/PAM	17.2 (−40°C)	−57.4	−40–RT	RuO_2/Co_3O_4	562 mA·hour g^{-1}	2 mA cm^{-2}	−40	(*120*)
						700.0 mA·hour g^{-1}		RT	
	IL/PAM	15.02 (RT)	*	RT–+50	$LiFePO_4$	142.9 mA·hour g^{-1}	28 mA g^{-1}	RT	(*84*)
	2 M $ZnSO_4$/0.1 $MnSO_4$ /H_2O/EG-waPUA/PAM	14.6 (−20°C)	~−25	−20–+20	α- MnO_2/CNT	226 mA·hour g^{-1}	0.2 A g^{-1}	−20	(*82*)
						275 mA·hour g^{-1}		20	
	2 M $ZnSO_4$ /0.2 M $MnSO_4$/PVA-B-G	10.1 (−35°C)	<−60	−35–+25	rGO/MnO_2	133.8 mA·hour g^{-1}	0.5 A g^{-1}	−35	(*121*)
						242.5 mA·hour g^{-1}		25	
	2 M $ZnSO_4$/0.1 $MnSO_4/H_2O$/GG	10.7 (RT)	*	+5–+45	MnO_2/rGO	113.5 mA·hour g^{-1}	3 A g^{-1}	5	(*122*)
						246.9 mA·hour g^{-1}		45	
	Zinc alginate gel	18.3 (RT)	*	0–+50	α-MnO_2/CNT	130 mA·hour g^{-1}	1 A g^{-1}	RT	(*21*)

continued on next page

Category	Electrolyte	Ionic conductivity (mS cm^{-1})	Freezing point (°C)	Operating temperature range (°C)	Cathode	Capacity of the full cell			Ref.
						Capacity	Current density	T (°C)	
	2 M $ZnSO_4$/0.1 M $MnSO_4$/H_2O/ locust bean gum	33.57 (RT)	*	0–+40	MnO_2/rGO	156.6 mA·hour g^{-1}	0.6 A g^{-1}	0	(*123*)
						235.6 mA·hour g^{-1}		20	
						319.1 mA·hour g^{-1}		40	
	1 M $Zn(OTf)_2$/ H_2O /PAM/ CNFs	6.8 (RT)	*	−18–+50	$Mg_{0.23}V_2O_5{\cdot}1.0H_2O$	330 mA·hour g^{-1}	0.5 A g^{-1}	RT	(*124*)
	2 M $ZnSO_4$ / H_2O /PZHE	32 (25°C), 83.5 (95°C)	*	−20–+25	VS_2	*	*	*	(*83*)
	30 wt % KOH/ H_2O/A-PAA	199 (−20°C)	~ −25	−20–+25	BFC-loaded air cathode	691 mA·hour g^{-1}	5 mA cm^{-2}	−20	(*20*)
	2 M $ZnSO_4$/0.2 M $MnSO_4$/H_2O/ elastomer-coated EG- alginate/ PAM	14.1 (−20°C) 18.2 (80°C)	−30–−20	−20–+80	MnO_2	165 mA·hour g^{-1}	0.2 A g^{-1}	-20	*(86)*
						272 mA·hour g^{-1}	0.1 A g^{-1}	25	
						105 mA·hour g^{-1}	2 A g^{-1}	80	
	6 M KOH/H_2O/ G-CyBA/PAM SP-DN	571.1 (RT), 252.2(−50°C), 63.2 (−80°C), 431.7 (100°C)	−196	−50–+100	air cathode	620 mA·hour g^{-1}	5 mA cm^{-2}	−50	(*85*)

welectrolytes for metal anode protection, while current study of their intrinsic properties to address the practical issues is lagging. In this respect, it is urgent to develop cost-effective electrolytes and, in the meanwhile, to show their promise under extended temperatures. This review has mainly targeted temperature adaptation strategies for zinc ion–based electrolytes, but it may also have reference value to other battery research beyond ZMBs, since the electrolytes share very similar fundamentals.

REFERENCES AND NOTES

1. Q. Zhang, Y. Ma, Y. Lu, L. Li, F. Wan, K. Zhang, J. Chen, Modulating electrolyte structure for ultralow temperature aqueous zinc batteries. *Nat. Commun.* **11**, 4463 (2020).
2. J. Hao, X. Li, X. Zeng, D. Li, J. Mao, Z. Guo, Deeply understanding the Zn anode behaviour and corresponding improvement strategies in different aqueous Zn-based batteries. *Energ. Environ. Sci.* **13**, 3917–3949 (2020).
3. X. Zeng, J. Hao, Z. Wang, J. Mao, Z. Guo, Recent progress and perspectives on aqueous Zn-based rechargeable batteries with mild aqueous electrolytes. *Energy Stor. Mater.* **20**, 410–437 (2019).
4. T. Sun, S. Zheng, H. Du, Z. Tao, Synergistic effect of cation and anion for low-temperature aqueous zinc-ion battery. *Nanomicro Lett.* **13**, 204 (2021).
5. L. Cao, D. Li, E. Hu, J. Xu, T. Deng, L. Ma, Y. Wang, X.-Q. Yang, C. Wang, Solvation structure design for aqueous Zn metal batteries. *J. Am. Chem. Soc.* **142**, 21404–21409 (2020).
6. S. Liu, J. Mao, W. K. Pang, J. Vongsvivut, X. Zeng, L. Thomsen, Y. Wang, J. Liu, D. Li, Z. Guo, Tuning the electrolyte solvation structure to suppress cathode dissolution, water reactivity, and Zn dendrite growth in zinc-ion batteries. *Adv. Funct. Mater.* **31**, 2104281 (2021).
7. X. Fan, X. Ji, L. Chen, J. Chen, T. Deng, F. Han, J. Yue, N. Piao, R. Wang, X. Zhou, X. Xiao, L. Chen, C. Wang, All-temperature batteries enabled by fluorinated electrolytes with non-polar solvents. *Nat. Energy* **4**, 882–890 (2019).
8. Y. Zhao, Z. Chen, F. Mo, D. Wang, Y. Guo, Z. Liu, X. Li, Q. Li, G. Liang, C. Zhi, Aqueous rechargeable metal-ion batteries working at subzero temperatures. *Adv. Sci.* **8**, 2002590 (2020).
9. F. Yue, Z. Tie, S. Deng, S. Wang, M. Yang, Z. J. Niu, Ultralow temperature aqueous battery with proton chemistry. *Angew. Chem. Int. Ed.* **60**, 13882–13886 (2021).
10. X. Dong, Z. Guo, Z. Guo, Y. Wang, Y. Xia, Organic batteries operated at −70°C. *Joule* **2**, 902–913 (2018).
11. N. Wang, X. Dong, B. Wang, Z. Guo, Z. Wang, R. Wang, X. Qiu, Y. Wang, Zinc–organic battery with a wide operation-temperature window from −70 to 150°C. *Angew. Chem. Int. Ed.* **132**, 14685–14691 (2020).
12. Q. Li, G. Liu, H. Cheng, Q. Sun, J. Zhang, J. Ming, Low-temperature electrolyte design for lithium-ion batteries: Prospect and challenges. *Chem. A Eur. J.* **27**, 15842–15865 (2021).
13. N. Zhang, Y. Dong, M. Jia, X. Bian, Y. Wang, M. Qiu, J. Xu, Y. Liu, L. Jiao, F. Cheng, Rechargeable aqueous Zn–V_2O_5 battery with high energy density and long cycle life. *ACS Energy Lett.* **3**, 1366–1372 (2018).
14. B. Tang, J. Zhou, G. Fang, F. Liu, C. Zhu, C. Wang, A. Pan, S. Liang, Engineering the interplanar spacing of ammonium vanadates as a high-performance aqueous zinc-ion battery cathode. *J. Mater. Chem. A* **7**, 940–945 (2019).
15. M. Zhu, X. Wang, H. Tang, J. Wang, Q. Hao, L. Liu, Y. Li, K. Zhang, O. G. Schmidt, Antifreezing hydrogel with high zinc reversibility for flexible and durable aqueous batteries by cooperative hydrated cations. *Adv. Funct. Mater.* **30**, 1907218 (2020).
16. T. Sun, X. Yuan, K. Wang, S. Zheng, J. Shi, Q. Zhang, W. Cai, J. Liang, Z. Tao, An ultralow-temperature aqueous zinc-ion battery. *J. Mater. Chem. A* **9**, 7042–7047 (2021).
17. N. Patil, C. Cruz, D. Ciurduc, A. Mavrandonakis, J. Palma, R. Marcilla, An ultrahigh performance zinc-organic battery using poly(catechol) cathode in $Zn(TFSI)_2$-based concentrated aqueous electrolytes. *Adv. Energy Mater.* **11**, 2100939 (2021).
18. W. Deng, Z. Zhou, Y. Li, M. Zhang, X. Yuan, J. Hu, Z. Li, C. Li, R. Li, High-capacity layered magnesium vanadate with concentrated gel electrolyte toward high-performance and wide-temperature zinc-ion battery. *ACS Nano* **14**, 15776–15785 (2020).
19. M. Chen, J. Chen, W. Zhou, X. Han, Y. Yao, C. P. Wong, Realizing an all-round hydrogel electrolyte toward environmentally adaptive dendrite-free aqueous Zn-MnO_2 batteries. *Adv. Mater. Interfaces* **33**, 2007559 (2021).
20. Z. Pei, Z. Yuan, C. Wang, S. Zhao, J. Fei, L. Wei, J. Chen, C. Wang, R. Qi, Z. Liu, Y. Chen, A flexible rechargeable zinc-air battery with excellent low-temperature adaptability. *Angew. Chem. Int. Ed.* **59**, 4793–4799 (2020).
21. Y. Tang, C. Liu, H. Zhu, X. Xie, J. Gao, C. Deng, M. Han, S. Liang, J. Zhou, Ion-confinement effect enabled by gel electrolyte for highly reversible dendrite-free zinc metal anode. *Energy Stor. Mater.* **27**, 109–116 (2020).
22. Z. Chen, T. Liu, Z. Zhao, Z. Zhang, X. Han, P. Han, J. Li, J. Wang, J. Li, S. Huang, X. Zhou, J. Zhao, G. Cui, Fast anion intercalation into graphite cathode enabling high-rate rechargeable zinc batteries. *J. Power Sources* **457**, 227994 (2020).
23. N. Chang, T. Li, R. Li, S. Wang, Y. Yin, H. Zhang, X. Li, An aqueous hybrid electrolyte for low-temperature zinc-based energy storage devices. *Energ. Environ. Sci.* **13**, 3527–3535 (2020).
24. J. Hao, L. Yuan, C. Ye, D. Chao, K. Davey, Z. Guo, S. Z. Qiao, Boosting zinc electrode reversibility in aqueous electrolytes by using low-cost antisolvents. *Angew. Chem. Int. Ed.* **60**, 7366–7375 (2021).
25. A. Naveed, H. Yang, J. Yang, Y. Nuli, J. Wang, Highly reversible and rechargeable safe Zn batteries based on a triethyl phosphate electrolyte. *Angew. Chem. Int. Ed.* **131**, 2786–2790 (2019).
26. A. Naveed, H. Yang, Y. Shao, J. Yang, N. Yanna, J. Liu, S. Shi, L. Zhang, A. Ye, B. He, J. Wang, A highly reversible Zn anode with intrinsically safe organic electrolyte for long-cycle-life batteries. *Adv. Mater.* **31**, 1900668 (2019).
27. N. Wang, Y. Yang, X. Qiu, X. Dong, Y. Wang, Y. Xia, Stabilized rechargeable aqueous zinc batteries using ethylene glycol as water blocker. *ChemSusChem* **13**, 5556–5564 (2020).
28. Y. You, H. R. Yao, S. Xin, Y. X. Yin, T. T. Zuo, C. P. Yang, Y. G. Guo, Y. Cui, L. J. Wan, J. B. Goodenough, Subzero-temperature cathode for a sodium-ion battery. *Adv. Mater.* **28**, 7243–7248 (2016).
29. K. Liu, Y. Liu, D. Lin, A. Pei, Y. Cui, Materials for lithium-ion battery safety. *Sci. Adv.* **4**, eaas9820 (2018).
30. Y. Nagata, K. Usui, M. Bonn, Molecular mechanism of water evaporation. *Phys. Rev. Lett.* **115**, 236102 (2015).
31. H. Wang, Z. Chen, Z. Ji, P. Wang, J. Wang, W. Ling, Y. Huang, Temperature adaptability issue of aqueous rechargeable batteries. *Mater. Today Energy* **19**, 100577 (2021).
32. R. Schulz, Y. von Hansen, J. O. Daldrop, J. Kappler, F. Noe, R. R. Netz, Collective hydrogen-bond rearrangement dynamics in liquid water. *J. Chem. Phys.* **149**, 244504 (2018).
33. S. Chakrabarty, E. R. Williams, The effect of halide and iodate anions on the hydrogen-bonding network of water in aqueous nanodrops. *Phys. Chem. Chem. Phys.* **18**, 25483–25490 (2016).
34. Y. Z. Zheng, Y. Zhou, Q. Liang, D. F. Chen, R. Guo, A theoretical study on the hydrogen-bonding interactions between flavonoids and ethanol/water. *J. Mol. Model.* **22**, 95 (2016).
35. Q. Zhang, K. Xia, Y. Ma, Y. Lu, L. Li, J. Liang, S. Chou, J. Chen, Chaotropic anion and fast-kinetics cathode enabling low-temperature aqueous Zn batteries. *ACS Energy Lett.* **6**, 2704–2712 (2021).
36. D. Reber, R.-S. Kühnel, C. Battaglia, Suppressing crystallization of water-in-salt electrolytes by asymmetric anions enables low-temperature operation of high-voltage aqueous batteries. *ACS Mater. Lett.* **1**, 44–51 (2019).
37. M. Becker, R. S. Kuhnel, C. Battaglia, Water-in-salt electrolytes for aqueous lithium-ion batteries with liquidus temperatures below −10°C. *Chem. Commun.* **55**, 12032–12035 (2019).
38. D. Reber, N. Takenaka, R. S. Kuhnel, A. Yamada, C. Battaglia, Impact of anion asymmetry on local structure and supercooling behavior of water-in-salt electrolytes. *J. Phys. Chem. Lett.* **11**, 4720–4725 (2020).
39. S. Cai, X. Chu, C. Liu, H. Lai, H. Chen, Y. Jiang, F. Guo, Z. Xu, C. Wang, C. Gao, Water-salt oligomers enable supersoluble electrolytes for high-performance aqueous batteries. *Adv. Mater.* **33**, 2007470 (2021).
40. Y. Yang, Y. Yang, Y. Cao, X. Wang, Y. Chen, H. Liu, Y. Gao, J. Wang, C. Liu, W. Wang, J.-K. Yu, D. Wu, Anti-freezing, resilient and tough hydrogels for sensitive and large-range strain and pressure sensors. *Chem. Eng. J.* **403**, 126431 (2021).
41. L. Suo, O. Borodin, W. Sun, X. Fan, C. Yang, F. Wang, T. Gao, Z. Ma, M. Schroeder, A. von Cresce, S. M. Russell, M. Armand, A. Angell, K. Xu, C. Wang, Advanced high-voltage aqueous lithium-ion battery enabled by "water-in-bisalt" electrolyte. *Angew. Chem. Int. Ed.* **55**, 7136–7141 (2016).
42. Y. Yamada, K. Usui, K. Sodeyama, S. Ko, Y. Tateyama, A. Yamada, Hydrate-melt electrolytes for high-energy-density aqueous batteries. *Nat. Energy* **1**, 16129 (2016).
43. M. R. Lukatskaya, J. I. Feldblyum, D. G. Mackanic, F. Lissel, D. L. Michels, Y. Cui, Z. Bao, Concentrated mixed cation acetate "water-in-salt" solutions as green and low-cost high voltage electrolytes for aqueous batteries. *Energ. Environ. Sci.* **11**, 2876–2883 (2018).
44. C. Zhang, J. Holoubek, X. Wu, A. Daniyar, L. Zhu, C. Chen, D. P. Leonard, I. A. Rodriguez-Perez, J. X. Jiang, C. Fang, X. Ji, A $ZnCl_2$ water-in-salt electrolyte for a reversible Zn metal anode. *Chem. Commun.* **54**, 14097–14099 (2018).
45. C. X. Zhao, J. N. Liu, N. Yao, J. Wang, D. Ren, X. Chen, B. Q. Li, Q. Zhang, Can aqueous zinc-air batteries work at sub-zero temperatures? *Angew. Chem. Int. Ed. Engl.* **60**, 15281–15285 (2021).
46. F. Wang, O. Borodin, T. Gao, X. Fan, W. Sun, F. Han, A. Faraone, J. A. Dura, K. Xu, C. Wang, Highly reversible zinc metal anode for aqueous batteries. *Nat. Mater.* **17**, 543–549 (2018).
47. L. Wang, S. Yan, C. D. Quilty, J. Kuang, M. R. Dunkin, S. N. Ehrlich, L. Ma, K. J. Takeuchi, E. S. Takeuchi, A. C. Marschilok, Achieving stable molybdenum oxide cathodes for aqueous zinc-ion batteries in water-in-salt electrolyte. *Adv. Mater. Interfaces* **8**, 2002080 (2021).

48. Y. Yamada, M. Yaegashi, T. Abe, A. Yamada, A superconcentrated ether electrolyte for fast-charging Li-ion batteries. *Chem. Commun.* **49**, 11194–11196 (2013).
49. L. Suo, Y. S. Hu, H. Li, M. Armand, L. Chen, A new class of solvent-in-salt electrolyte for high-energy rechargeable metallic lithium batteries. *Nat. Commun.* **4**, 1481 (2013).
50. H. Ao, C. Chen, Z. Hou, W. Cai, M. Liu, Y. Jin, X. Zhang, Y. Zhu, Y. Qian, Electrolyte solvation structure manipulation enables safe and stable aqueous sodium ion batteries. *J. Mater. Chem. A* **8**, 14190–14197 (2020).
51. Y. Luo, L. Wei, H. Geng, Y. Zhang, Y. Yang, C. C. Li, Amorphous bimetallic oxides Fe-V-O with tunable compositions toward rechargeable Zn-ion batteries with excellent low-temperature performance. *ACS Appl. Mater. Interfaces* **12**, 11753–11760 (2020).
52. H. Geng, M. Cheng, B. Wang, Y. Yang, Y. Zhang, C. C. Li, Electronic structure regulation of layered vanadium oxide via interlayer doping strategy toward superior high-rate and low-temperature zinc-ion batteries. *Adv. Funct. Mater.* **30**, 1907684 (2020).
53. C. Lin, F. Qi, H. Dong, X. Li, C. Shen, E. H. Ang, Y. Han, H. Geng, C. C. Li, Suppressing vanadium dissolution of V_2O_5 via in situ polyethylene glycol intercalation towards ultralong lifetime room/low-temperature zinc-ion batteries. *Nanoscale* **13**, 17040–17048 (2021).
54. Z. Chen, Y. Tang, X. Du, B. Chen, G. Lu, X. Han, Y. Zhang, W. Yang, P. Han, J. Zhao, G. Cui, Anion solvation reconfiguration enables high-voltage carbonate electrolytes for stable Zn/graphite cells. *Angew. Chem. Int. Ed. Engl.* **59**, 21769–21777 (2020).
55. X. Qiu, N. Wang, X. Dong, J. Xu, K. Zhou, W. Li, Y. Wang, A high-voltage Zn–organic battery using a nonflammable organic electrolyte. *Angew. Chem. Int. Ed.* **60**, 21025–21032 (2021).
56. Q. Li, S. Jiao, L. Luo, M. S. Ding, J. Zheng, S. S. Cartmell, C. M. Wang, K. Xu, J. G. Zhang, W. Xu, Wide-temperature electrolytes for lithium-ion batteries. *ACS Appl. Mater. Interfaces* **9**, 18826–18835 (2017).
57. R. Mogensen, A. Buckel, S. Colbin, R. Younesi, A wide-temperature-range, low-cost, fluorine-free battery electrolyte based on sodium bis(oxalate)borate. *Chem. Mater.* **33**, 1130–1139 (2021).
58. S. Lin, H. Hua, P. Lai, J. Zhao, A multifunctional dual-salt localized high-concentration electrolyte for fast dynamic high-voltage lithium battery in wide temperature range. *Adv. Energy Mater.* **11**, 2101775 (2021).
59. Y.-G. Cho, M. Li, J. Holoubek, W. Li, Y. Yin, Y. S. Meng, Z. Chen, Enabling the low-temperature cycling of NMC||graphite pouch cells with an ester-based electrolyte. *ACS Energy Lett.* **6**, 2016–2023 (2021).
60. W. Yang, X. Du, J. Zhao, Z. Chen, G. Cui, Hydrated eutectic electrolytes with ligand-oriented solvation shells for long-cycling zinc-organic batteries. *Joule* **4**, 1557–1574 (2020).
61. Y. Jin, K. S. Han, Y. Shao, M. L. Sushko, J. Xiao, H. Pan, J. Liu, Stabilizing zinc anode reactions by polyethylene oxide polymer in mild aqueous electrolytes. *Adv. Funct. Mater.* **30**, 2003932 (2020).
62. R. Qin, Y. Wang, M. Zhang, Y. Wang, S. Ding, A. Song, H. Yi, L. Yang, Y. Song, Y. Cui, J. Liu, Z. Wang, S. Li, Q. Zhao, F. Pan, Tuning Zn^{2+} coordination environment to suppress dendrite formation for high-performance Zn-ion batteries. *Nano Energy* **80**, 105478 (2021).
63. A. Wang, W. Zhou, A. Huang, M. Chen, Q. Tian, J. Chen, Developing improved electrolytes for aqueous zinc-ion batteries to achieve excellent cyclability and antifreezing ability. *J. Colloid Interface Sci.* **586**, 362–370 (2021).
64. H. Du, K. Wang, T. Sun, J. Shi, X. Zhou, W. Cai, Z. Tao, Improving zinc anode reversibility by hydrogen bond in hybrid aqueous electrolyte. *Chem. Eng. J.* **427**, 131705 (2022).
65. D. Feng, F. Cao, L. Hou, T. Li, Y. Jiao, P. Wu, Immunizing aqueous Zn batteries against dendrite formation and side reactions at various temperatures via electrolyte additives. *Small* **17**, 2103195 (2021).
66. Q. Nian, J. Wang, S. Liu, T. Sun, S. Zheng, Y. Zhang, Z. Tao, J. Chen, Aqueous batteries operated at −50°C. *Angew. Chem. Int. Ed.* **58**, 16994–16999 (2019).
67. A. P. Semenov, R. I. Mendgaziev, A. S. Stoporev, V. A. Istomin, D. V. Sergeeva, A. G. Ogienko, V. A. Vinokurov, The pursuit of a more powerful thermodynamic hydrate inhibitor than methanol. Dimethyl sulfoxide as a case study. *Chem. Eng. J.* **423**, 130227 (2021).
68. Q. Dou, S. Lei, D.-W. Wang, Q. Zhang, D. Xiao, H. Guo, A. Wang, H. Yang, Y. Li, S. Shi, X. Yan, Safe and high-rate supercapacitors based on an "acetonitrile/water in salt" hybrid electrolyte. *Energ. Environ. Sci.* **11**, 3212–3219 (2018).
69. X. Lu, J. M. Vicent-Luna, S. Calero, R. M. Madero-Castro, M. C. Gutiérrez, M. L. Ferrer, F. del Monte, $EMIMBF_4$ in ternary liquid mixtures of water, dimethyl sulfoxide and acetonitrile as "tri-solvent-in-salt" electrolytes for high-performance supercapacitors operating at −70°C. *Energy Stor. Mater.* **40**, 368–385 (2021).
70. D. Xu, Z. L. Wang, J. J. Xu, L. L. Zhang, X. B. Zhang, Novel DMSO-based electrolyte for high performance rechargeable Li-O_2 batteries. *Chem. Commun.* **48**, 6948–6950 (2012).
71. D. B. Wong, K. P. Sokolowsky, M. I. El-Barghouthi, E. E. Fenn, C. H. Giammanco, A. L. Sturlaugson, M. D. Fayer, Water dynamics in water/DMSO binary mixtures. *J. Phys. Chem. B* **116**, 5479–5490 (2012).
72. A. K. Sum, D. T. Wu, K. Yasuoka, Energy science of clathrate hydrates: Simulation-based advances. *MRS Bull.* **36**, 205–210 (2011).
73. A. G. Ogienko, V. A. Drebushchak, E. G. Bogdanova, A. S. Yunoshev, A. A. Ogienko, E. V. Boldyreva, A. Y. Manakov, Thermodynamic aspects of freeze-drying. *J. Therm. Anal. Calorim.* **127**, 1593–1604 (2017).
74. D.-Y. Kim, Y. Park, H. Lee, Tuning clathrate hydrates: Application to hydrogen storage. *Catal. Today* **120**, 257–261 (2007).
75. X. Zeng, J. Hao, J. Liu, S. Liu, Z. Wang, Y. Wang, S. Zhang, T. Zheng, J. Liu, P. Rao, Z. Guo, Electrolyte design for in situ construction of highly Zn^{2+}-conductive solid electrolyte interphase to enable high-performance aqueous Zn-ion batteries under practical conditions. *Adv. Mater.* **33**, 2007416 (2021).
76. X. Zeng, K. Xie, S. Liu, S. Zhang, J. Hao, J. Liu, W. K. Pang, J. Liu, P. Rao, Q. Wang, J. Mao, Z. Guo, Bio-inspired design of an in situ multifunctional polymeric solid-electrolyte interphase for Zn metal anode cycling at 30 mA cm^{-2} and 30 mA h cm^{-2}. *Energ. Environ. Sci.* **14**, 5947–5957 (2021).
77. D. Zhou, F. Chen, S. Handschuh-Wang, T. Gan, X. Zhou, X. Zhou, Biomimetic extreme-temperature- and environment-adaptable hydrogels. *ChemPhysChem* **20**, 2139–2154 (2019).
78. Z. Wang, H. Li, Z. Tang, Z. Liu, Z. Ruan, L. Ma, Q. Yang, D. Wang, C. Zhi, Hydrogel electrolytes for flexible aqueous energy storage devices. *Adv. Funct. Mater.* **28**, 1804560 (2018).
79. Y. Jian, S. Handschuh-Wang, J. Zhang, W. Lu, X. Zhou, T. Chen, Biomimetic anti-freezing polymeric hydrogels: Keeping soft-wet materials active in cold environments. *Mater. Horiz.* **8**, 351–369 (2021).
80. N. Sun, F. Lu, Y. Yu, L. Su, X. Gao, L. Zheng, Alkaline double-network hydrogels with high conductivities, superior mechanical performances, and antifreezing properties for solid-state zinc-air batteries. *ACS Appl. Mater. Interfaces* **12**, 11778–11788 (2020).
81. J. Wang, Y. Huang, B. Liu, Z. Li, J. Zhang, G. Yang, P. Hiralal, S. Jin, H. Zhou, Flexible and anti-freezing zinc-ion batteries using a guar-gum/sodium-alginate/ethylene-glycol hydrogel electrolyte. *Energy Stor. Mater.* **41**, 599–605 (2021).
82. F. Mo, G. Liang, Q. Meng, Z. Liu, H. Li, J. Fan, C. Zhi, A flexible rechargeable aqueous zinc manganese-dioxide battery working at −20°C. *Energ. Environ. Sci.* **12**, 706–715 (2019).
83. K. Leng, G. Li, J. Guo, X. Zhang, A. Wang, X. Liu, J. Luo, A safe polyzwitterionic hydrogel electrolyte for long-life quasi-solid state zinc metal batteries. *Adv. Funct. Mater.* **30**, 2001317 (2020).
84. J. Huang, X. Chi, Y. Du, Q. Qiu, Y. Liu, Ultrastable zinc anodes enabled by anti-dehydration ionic liquid polymer electrolyte for aqueous Zn batteries. *ACS Appl. Mater. Interfaces* **13**, 4008–4016 (2021).
85. C. Gu, X.-Q. Xie, Y. Liang, J. Li, H. Wang, K. Wang, J. Liu, M. Wang, Y. Zhang, M. Li, H. Kong, C.-S. Liu, Small molecule-based supramolecular-polymer double-network hydrogel electrolytes for ultra-stretchable and waterproof Zn–air batteries working from −50 to 100°C. *Energ. Environ. Sci.* **14**, 4451–4462 (2021).
86. F. Mo, G. Liang, D. Wang, Z. Tang, H. Li, C. Zhi, Biomimetic organohydrogel electrolytes for high-environmental adaptive energy storage devices. *EcoMat* **1**, e12008 (2019).
87. C. Pan, R. Zhang, R. G. Nuzzo, A. A. Gewirth, $ZnNi_xMn_xCo_{2-2x}O_4$ spinel as a high-voltage and high-capacity cathode material for nonaqueous Zn-ion batteries. *Adv. Energy Mater.* **8**, 1800589 (2018).
88. X. Jia, C. Liu, Z. G. Neale, J. Yang, G. Cao, Active materials for aqueous zinc ion batteries: Synthesis, crystal structure, morphology, and electrochemistry. *Chem. Rev.* **120**, 7795–7866 (2020).
89. L. Cao, D. Li, F. A. Soto, B. Zhang, V. Ponce, L. Ma, T. Deng, J. M. Seminario, E. Hu, X. Q. Yang, P. B. Balbuena, C. Wang, Highly reversible aqueous Zn batteries enabled by zincophilic-zincophobic interfacial layer and interrupted hydrogen bond electrolyte. *Angew. Chem. Int. Ed.* **133**, 18993–18999 (2021).
90. S. Chen, Y. Zhang, H. Geng, Y. Yang, X. Rui, C. C. Li, Zinc ions pillared vanadate cathodes by chemical pre-intercalation towards long cycling life and low-temperature zinc ion batteries. *J. Power Sources* **441**, 227192 (2019).
91. T. He, Y. Ye, H. Li, S. Weng, Q. Zhang, M. Li, T. Liu, J. Cheng, X. Wang, J. Lu, B. Wang, Oxygen-deficient ammonium vanadate for flexible aqueous zinc batteries with high energy density and rate capability at −30°C. *Mater. Today* **43**, 53–61 (2021).
92. G. Su, S. Chen, H. Dong, Y. Cheng, Q. Liu, H. Wei, E. H. Ang, H. Geng, C. C. Li, Tuning the electronic structure of layered vanadium pentoxide by pre-intercalation of potassium ions for superior room/low-temperature aqueous zinc-ion batteries. *Nanoscale* **13**, 2399–2407 (2021).
93. X. Cui, J. Lee, K. R. Ng, W. N. Chen, Food waste durian rind-derived cellulose organohydrogels: Toward anti-freezing and antimicrobial wound dressing. *ACS Sustainable Chem. Eng.* **9**, 1304–1312 (2021).
94. N. Yesibolati, N. Umirov, A. Koishybay, M. Omarova, I. Kurmanbayeva, Y. Zhang, Y. Zhao, Z. Bakenov, High performance Zn/$LiFePO_4$ aqueous rechargeable battery for large scale applications. *Electrochim. Acta* **152**, 505–511 (2015).

95. J.-Q. Huang, X. Lin, H. Tan, X. Du, B. Zhang, Realizing high-performance Zn-ion batteries by a reduced graphene oxide block layer at room and low temperatures. *J. Energy Chem.* **43**, 1–7 (2020).
96. D. Han, C. Cui, K. Zhang, Z. Wang, J. Gao, Y. Guo, Z. Zhang, S. Wu, L. Yin, Z. Weng, F. Kang, Q.-H. Yang, A non-flammable hydrous organic electrolyte for sustainable zinc batteries. *Nat. Sustain.*, (2021).
97. X. Lin, G. Zhou, M. J. Robson, J. Yu, S. C. T. Kwok, F. Ciucci, Hydrated deep eutectic electrolytes for high-performance Zn-ion batteries capable of low-temperature operation. *Adv. Funct. Mater.*, 2109322 (2021).
98. T. Wei, Y. Peng, L. Mo, S. Chen, R. Ghadari, Z. Li, L. Hu, Modulated bonding interaction in propanediol electrolytes toward stable aqueous zinc-ion batteries. *Sci. China Mater.*, (2021).
99. J. Wang, Q. Zhu, F. Li, J. Chen, H. Yuan, Y. Li, P. Hu, M. S. Kurbanov, H. Wang, Low-temperature and high-rate Zn metal batteries enabled by mitigating Zn^{2+} concentration polarization. *Chem. Eng. J.* **433**, 134589 (2022).
100. J. Shi, S. Wang, X. Chen, Z. Chen, X. Du, T. Ni, Q. Wang, L. Ruan, W. Zeng, Z. Huang, An ultrahigh energy density quasi-solid-state zinc ion microbattery with excellent flexibility and thermostability. *Adv. Energy Mater.* **9**, 1901957 (2019).
101. L. Li, W. Liu, H. Dong, Q. Gui, Z. Hu, Y. Li, J. Liu, Surface and interface engineering of nanoarrays toward advanced electrodes and electrochemical energy storage devices. *Adv. Mater.* **33**, e2004959 (2021).
102. J. Zhao, W. Wu, X. Jia, T. Xia, Q. Li, J. Zhang, Q. Wang, W. Zhang, C. Lu, High-value utilization of biomass waste: From garbage floating on the ocean to high-performance rechargeable Zn–MnO_2 batteries with superior safety. *J. Mater. Chem. A* **8**, 18198–18206 (2020).
103. Y. Jiang, D. Ba, Y. Li, J. Liu, Noninterference revealing of "layered to layered" zinc storage mechanism of δ- MnO_2 toward neutral Zn-Mn batteries with superior performance. *Adv. Sci.* **7**, 1902795 (2020).
104. D. Lou, C. Wang, Z. He, X. Sun, J. Luo, J. Li, Robust organohydrogel with flexibility and conductivity across the freezing and boiling temperatures of water. *Chem. Commun.* **55**, 8422–8425 (2019).
105. L. Ma, N. Li, C. Long, B. Dong, D. Fang, Z. Liu, Y. Zhao, X. Li, J. Fan, S. Chen, S. Zhang, C. Zhi, Achieving both high voltage and high capacity in aqueous zinc-ion battery for record high energy density. *Adv. Funct. Mater.* **29**, 1906142 (2019).
106. H. Zhang, X. Liu, H. Li, B. Qin, S. Passerini, High-voltage operation of a V_2O_5 cathode in a concentrated gel polymer electrolyte for high-energy aqueous zinc batteries. *ACS Appl. Mater. Interfaces* **12**, 15305–15312 (2020).
107. C. Yan, Y. Wang, Z. Chen, X. Deng, Hygroscopic double-layer gel polymer electrolyte toward high-performance low-temperature zinc hybrid batteries. *Batteries Supercaps* **4**, 1627–1635 (2021).
108. Y. Chen, J. Zhao, Y. Wang, Quasi-solid-state zinc ion rechargeable batteries for subzero temperature applications. *ACS Appl. Energy Mater.* **3**, 9058–9065 (2020).
109. Y. Wang, Y. Chen, A flexible zinc-ion battery based on the optimized concentrated hydrogel electrolyte for enhanced performance at subzero temperature. *Electrochim. Acta* **395**, 139178 (2021).
110. Y. Liu, X. Zhou, Y. Bai, R. Liu, X. Li, H. Xiao, Y. Wang, X. Wang, Y. Ma, G. Yuan, Engineering integrated structure for high-performance flexible zinc-ion batteries. *Chem. Eng. J.* **417**, 127955 (2020).
111. L. Li, S. Liu, W. Liu, D. Ba, W. Liu, Q. Gui, Y. Chen, Z. Hu, Y. Li, J. Liu, Electrolyte concentration regulation boosting zinc storage stability of high-capacity $K_{0.486}V_2O_5$ cathode for bendable quasi-solid-state zinc ion batteries. *Nanomicro Lett.* **13**, 34 (2021).
112. H. Wang, J. Liu, J. Wang, M. Hu, Y. Feng, P. Wang, Y. Wang, N. Nie, J. Zhang, H. Chen, Q. Yuan, J. Wu, Y. Huang, Concentrated hydrogel electrolyte-enabled aqueous rechargeable NiCo//Zn battery working from −20 to 50°C. *ACS Appl. Mater. Interfaces* **11**, 49–55 (2019).
113. Q. Wang, X. Pan, H. Zhang, S. Cao, X. Ma, L. Huang, L. Chen, Y. Ni, Fruit-battery-inspired self-powered stretchable hydrogel-based ionic skin that works effectively in extreme environments. *J. Mater. Chem. A* **9**, 3968–3975 (2021).
114. W. Zhou, J. Chen, M. Chen, A. Wang, A. Huang, X. Xu, J. Xu, C.-P. Wong, An environmentally adaptive quasi-solid-state zinc-ion battery based on magnesium vanadate hydrate with commercial-level mass loading and anti-freezing gel electrolyte. *J. Mater. Chem. A* **8**, 8397–8409 (2020).
115. G. Chen, J. Huang, J. Gu, S. Peng, X. Xiang, K. Chen, X. Yang, L. Guan, X. Jiang, L. Hou, Highly tough supramolecular double network hydrogel electrolytes for an artificial flexible and low-temperature tolerant sensor. *J. Mater. Chem. A* **8**, 6776–6784 (2020).
116. Z. Cong, W. Guo, P. Zhang, W. Sha, Z. Guo, C. Chang, F. Xu, X. Gang, W. Hu, X. Pu, Wearable antifreezing fiber-shaped Zn/PANI batteries with suppressed Zn dendrites and operation in sweat electrolytes. *ACS Appl. Mater. Interfaces* **13**, 17608–17617 (2021).
117. Y. Quan, M. Chen, W. Zhou, Q. Tian, J. Chen, High-performance anti-freezing flexible Zn-MnO_2 battery based on polyacrylamide/graphene oxide/ethylene glycol gel electrolyte. *Front. Chem.* **8**, 603 (2020).
118. X. Li, H. Wang, X. Sun, J. Li, Y.-N. Liu, Flexible wide-temperature zinc-ion battery enabled by an ethylene glycol-based organohydrogel electrolyte. *ACS Appl. Energy Mater.* **4**, 12718–12727 (2021).
119. X. Jin, L. Song, C. Dai, H. Ma, Y. Xiao, X. Zhang, Y. Han, X. Li, J. Zhang, Y. Zhao, Z. Zhang, L. Duan, L. Qu, A self-healing zinc ion battery under −20°C. *Energy Stor. Mater.* **44**, 517–526 (2022).
120. D. Jiang, H. Wang, S. Wu, X. Sun, J. Li, Flexible zinc–air battery with high energy efficiency and freezing tolerance enabled by DMSO-based organohydrogel electrolyte. *Small Methods* **6**, 2101043 (2022).
121. M. Chen, W. Zhou, A. Wang, A. Huang, J. Chen, J. Xu, C.-P. Wong, Anti-freezing flexible aqueous Zn–MnO_2 batteries working at -35°C enabled by a borax-crosslinked polyvinyl alcohol/glycerol gel electrolyte. *J. Mater. Chem. A* **8**, 6828–6841 (2020).
122. Y. Huang, J. Zhang, J. Liu, Z. Li, S. Jin, Z. Li, S. Zhang, H. Zhou, Flexible and stable quasi-solid-state zinc ion battery with conductive guar gum electrolyte. *Mater. Today Energy* **14**, 100349 (2019).
123. B. Liu, Y. Huang, J. Wang, Z. Li, G. Yang, S. Jin, E. Iranmanesh, P. Hiralal, H. Zhou, Highly conductive locust bean gum bio-electrolyte for superior long-life quasi-solid-state zinc-ion batteries. *RSC Adv.* **11**, 24862–24871 (2021).
124. W. Xu, C. Liu, Q. Wu, W. Xie, W.-Y. Kim, S.-Y. Lee, J. Gwon, A stretchable solid-state zinc ion battery based on a cellulose nanofiber–polyacrylamide hydrogel electrolyte and a $Mg_{0.23}V_2O_5{\cdot}1.0H_2O$ cathode. *J. Mater. Chem. A* **8**, 18327–18337 (2020).

Acknowledgments

Funding: This work was supported by an Australian Research Council Discovery Project (DP200101862 and FL210100050). **Author contributions:** Z.G. and S.L. conceived the topic of the review. R.Z. and S.L. wrote the manuscript and contributed equally to the content. Z.G., J.M., and Q.C. edited and reviewed the paper before submission. All the authors contributed to discussions of the manuscript. **Competing interests**: The authors declare that they have no competing interests. **Data and materials availability:** All data needed to evaluate the conclusions in the paper are presented in the paper.

Submitted 1 December 2021
Accepted 1 February 2022
Published 23 March 2022
10.1126/sciadv.abn5097